Article

Intestinal macrophages modulate synucleinopathy along the gut–brain axis

https://doi.org/10.1038/s41586-025-09984-y

Received: 23 October 2023

Accepted: 1 December 2025

Published online: 28 January 2026

Open access

Check for updates

Sebastiaan De Schepper[1,19]✉, Viktoras Konstantellos[1], James A. Conway[1,20], Dimitra Sokolova[1,20], Ludovica Zaccagnini[1], Matthew V. Cowley[2], Annerieke Sierksma[3,4], Maria Yudina[1], Marisa Edmonds[1], Daria Gavriouchkina[1], Bethany Geary[5], Amber Wallis[1], Meral Celikag[1], Zeynep Baykam[1], Mónica Vara-Pérez[6,7,8], Gerard Crowley[1], Fabian Tobias Hager[9], Mitchell Bijnen[10], David Posner[11,12], Kelvin Luk[13], Vuk Cerovic[9], Menna Clatworthy[11,12,14], Elizabeth J. Videlock[15], Zane Jaunmuktane[16,17], Kiavash Movahedi[6,7], Melanie Greter[10], Benny Chain[2,18], Dario R. Alessi[5], Soyon Hong[1,21]✉ & Tim Bartels[1,21]✉

Emerging evidence suggests that Parkinson's disease (PD) may have its origin in the enteric nervous system (ENS), from where α-synuclein (αS) pathology spreads to the brain[1–4]. Decades before the onset of motor symptoms, patients with PD suffer from constipation and present with circulating T cells responsive to αS, suggesting that peripheral immune responses initiated in the ENS may be involved in the early stages of PD[1,5–7]. However, cellular mechanisms that trigger αS pathology in the ENS and its spread along the gut–brain axis remain elusive. Here we demonstrate that muscularis macrophages (ME-Macs), housekeepers of ENS integrity and intestinal homeostasis, modulate αS pathology and neurodegeneration in models of PD[8,9]. ME-Macs contain misfolded αS, adopt a signature reflecting endolysosomal dysfunction and modulate the expansion of T cells that travel from the ENS to the brain through the dura mater as αS pathology progresses. Directed ME-Mac depletion leads to reduced αS pathology in the ENS and central nervous system, prevents T cell expansion and mitigates neurodegeneration and motor dysfunction, suggesting a role for ME-Macs as early cellular initiators of αS pathology along the gut–brain axis. Understanding these mechanisms could pave the way for early-stage biomarkers in PD.

There is growing awareness that the ENS may represent the initial site of αS pathology in PD. Constipation is one of the earliest and most common symptoms in patients with PD and probably reflects ENS dysfunction[1,10]. The concept of body-first PD is strongly supported by post-mortem and multimodal imaging studies showing early Lewy pathology in the ENS of patients with PD, suggesting a caudo-rostral distribution from the intestine to the brainstem and other brain regions[2,11]. Further, intestinal injections of αS in mice result in the hierarchical spread of Lewy pathology to the brain, strongly implicating the ENS in early stages of disease[3,4]. However, little is known about the cellular and molecular mechanisms that could trigger the onset of αS pathology in the ENS and progression to the brain.

Tissue-resident macrophages are specialized phagocytes that orchestrate numerous niche-specific functions critical for tissue homeostasis[12]. In the intestine, macrophages facing the microbiota are continually replaced by blood monocytes and are strategically positioned in the murine lamina propria to engulf penetrating pathogens[13]. By contrast, ME-Macs reside in the muscularis externa (ME) and support the functional integrity of the myenteric plexus, a network of enteric neurons integral to gastrointestinal motility[8,9,14]. ME-Macs colonize the murine intestine before birth, are self-maintained but gradually replaced throughout life and maintain enteric neuronal health through the production of neurotrophic factors and the clearance of debris. In the ageing murine intestine, ME-Macs accumulate αS and express

[1]UK Dementia Research Institute, University College London, London, UK. [2]Division of Infection and Immunity, University College London, London, UK. [3]VIB Center for Brain and Disease Research, Leuven, Belgium. [4]Laboratory for the Research of Neurodegenerative Diseases, Department of Neurosciences, Leuven Brain Institute, KU Leuven, Leuven, Belgium. [5]Medical Research Council (MRC) Protein Phosphorylation and Ubiquitylation Unit, School of Life Sciences, University of Dundee, Dundee, UK. [6]Brain and Systems Immunology Laboratory, Vrije Universiteit Brussel, Brussels, Belgium. [7]Brussels Center for Immunology, Vrije Universiteit Brussel, Brussels, Belgium. [8]Myeloid Cell Immunology Laboratory, VIB Center for Inflammation Research, Brussels, Belgium. [9]Institute of Molecular Medicine, RWTH Aachen University, Aachen, Germany. [10]Institute of Experimental Immunology, University of Zurich, Zurich, Switzerland. [11]Molecular Immunity Unit, Department of Medicine, University of Cambridge, Cambridge, UK. [12]Cambridge Institute for Therapeutic Immunology and Infectious Diseases, University of Cambridge, Cambridge, UK. [13]Department of Pathology and Laboratory Medicine, Institute on Aging and Center for Neurodegenerative Disease Research, Perelman School of Medicine at the University of Pennsylvania, Philadelphia, PA, USA. [14]Cellular Genetics, Wellcome Sanger Institute, Hinxton, UK. [15]Center for Inflammatory Bowel Diseases, Vatche and Tamar Manoukian Division of Digestive Diseases, David Geffen School of Medicine, UCLA, Los Angeles, CA, USA. [16]Department of Clinical and Movement Neurosciences, UCL Queen Square Institute of Neurology, London, UK. [17]Queen Square Brain Bank for Neurological Disorders, UCL Queen Square Institute of Neurology, London, UK. [18]Department of Computer Science, University College London, London, UK. [19]Present address: VIB Center for Molecular Neurology, University of Antwerp, Antwerp, Belgium. [20]These authors contributed equally: James A. Conway, Dimitra Sokolova. [21]These authors jointly supervised this work: Soyon Hong, Tim Bartels. ✉e-mail: sebastiaan.deschepper@uantwerpen.be; soyon.hong@ucl.ac.uk; t.bartels@ucl.ac.uk

PD-associated genes *Gba1* and *Lrrk2*, raising the intriguing question of whether ME-Macs could confer risk in body-first PD pathology[15]. Whereas central nervous system (CNS)-resident macrophages have been implicated in αS pathology, the role of ENS-resident ME-Macs remains unclear[7,16,17].

Here we show that ME-Macs are necessary for the formation and distribution of αS pathology in the intestine and the CNS. In mouse models of PD, including αS transgenic mice and ME injections of patient-derived-αS, ME-Macs, but not enteric neurons, contain misfolded, aggregated αS that coincides with endolysosomal activation in ME-Macs. Mechanistically, we found that ME-Macs in PD mouse models modulate T cell expansion in the ENS. We further show that T cells invade the CNS as αS pathology progresses, and preventing T cell egression ameliorated neurodegeneration. Functionally, we show that injection of anti-CSF1R with anti-CCR2 into the ME, targeting ME-Macs, ameliorated αS pathology in both the ENS and CNS, abolished T cell migration along the gut–brain axis and improved motor defects and neurodegeneration in mouse models of synucleinopathy. Together, our results uncover the role of ME-Macs in the onset and progression of αS pathology and motor impairments along the gut–brain axis in body-first PD.

ME-Macs engulf and modify αS pathology

We first investigated the onset of αS pathology in the ENS versus CNS in 3KL αS transgenic mice, in which αS expression is driven by Thy1 and the 3K construct introduces phenotypic amplification of familial E46K mutations promoting αS tetramer destabilization and aggregation[18]. 3KL mice demonstrate key features of PD pathology including progressive cortical pathological αS, hereafter defined as s129p$^+$ αS, selective neuronal loss and L-DOPA responsive motor impairments at 8 months of age[18]. Immunohistochemistry (IHC) on mechanically separated duodenal ME demonstrated significantly increased s129p$^+$ αS surrounding HuC/D$^+$ myenteric ganglia, a specialized group of enteric neurons within the ME, of 3KL versus wild-type (WT) mice (Fig. 1a–c) at 3 months. We focused on the duodenum, a region highly innervated by the vagus nerve. We also observed s129p$^+$ αS in the ME of postmortem PD tissues (Extended Data Fig. 1a,b). Further, increased total gut transit time was observed in 3-month 3KL versus WT, suggesting impaired ENS function and constipation (Fig. 1d). However, we found no changes in murine myenteric ganglia and glial volume, measured by HUC/D and glial fibrillary acidic protein, indicating the absence of neuronal death despite αS and enteric pathology (Extended Data Fig. 1c,d). To investigate underlying molecular changes, we performed digital spatial profiling (DSP) on duodenal myenteric plexus in 3-month 3KL versus WT mice using a multiplexed antibody panel consisting of PD-associated targets (Fig. 1e). We observed increased expression of proteins related to autophagy and lysosomal biology in myenteric ganglia of 3KL versus WT, including PINK1, LRRK2 and VPS35 that are associated with familial PD (Fig. 1e). Of note, DSP confirmed upregulation of s129p$^+$ αS in myenteric plexus and elevated total αS levels in both the lamina propria and myenteric plexus (Extended Data Fig. 1e). In the brain, we observed increased punctate αS s129p$^+$ staining in cholinergic neurons of the dorsal motor nucleus of the vagus of 3KL animals at 6 months compared with age-matched WT controls (Extended Data Fig. 1f–k).

Inflammation has been linked to the initiation and progression of αS pathology, and many PD risk genes are enriched in immune cells[7,19]. Macrophages are the most abundant innate immune cells in the intestinal layers. ME-Macs have a crucial role in maintaining ENS integrity, with their loss leading to constipation[8,9,14]. We observed no significant differences in ME-Mac distribution across the duodenum, jejunum and ileum of 3-month WT versus 3KL animals (Extended Data Fig. 2a,b). Fluorescence-activated cell sorting (FACS) analysis of ME and lamina propria revealed unaltered differentiation of intestinal macrophages from monocyte precursors at 3 months, 4 months and 6 months of age[13] (Extended Data Fig. 2c–f). By contrast, ME-Macs demonstrated increased expression levels of CSF1R and major histocompatibility complex class II (MHCII) (Extended Data Fig. 2g). We questioned whether ME-Macs, as professional phagocytes of the ENS, engage in the clearance of accumulating αS in surrounding myenteric neurons (Fig. 1f–j and Extended Data Fig. 2h,i). We assessed levels of lysosomal LAMP1 in ME-Macs and found an almost twofold increase in LAMP1 expression in ME-Macs from 3KL versus WT (Fig. 1h). We observed a roughly 14-fold increase in s129p$^+$ αS engulfment by ME-Macs (that is, in LAMP1$^+$ lysosomes) in 3-month 3KL mice compared with age-matched WT controls and a similar 14-fold increase in ME-Macs in postmortem jejunum of PD versus neurologically healthy control (NHC) participants (Fig. 1i,j and Supplementary Table 1a). Further, we found significant ($P \leq 0.05$) differential expression of 474 proteins using mass spectrometry in sorted CX3CR1^{hi}CD11c^{lo} ME-Macs of 3-month 3KL versus WT mice including lysosomal GRN, CTSB and CD68 (Fig. 1k and Extended Data Fig. 2k). Observed downregulated proteins included NDUFV3, NDUFB10, NDUFA4 and NDUFA7, part of the mitochondrial NADH-ubiquinone oxidoreductase complex that has been implicated in PD[20] (Fig. 1k). Notably, 3-month 3KL ME-Macs acquire signatures related to phagosome maturation and lysosome pathways (collectively referred to as the coordinated lysosomal expression and regulation network)[21], suggesting continuing clearance response in ME-Macs exposed to s129p$^+$ αS and confirming our DSP data (Fig. 1l and Extended Data Fig. 2j).

We then asked whether s129p$^+$ αS engulfed by 3KL ME-Macs shows altered pathological activity compared with WT ME-Macs and enteric neurons. We adapted the αS seed amplification assay (SAA) to isolated ME-Macs and enteric neurons to detect prion-like misfolded αS by means of templated aggregation of monomeric αS, which results in amplified binding to thioflavin T[22] (Fig. 1m). Notably, lysates from isolated ME-Macs of 3-month 3KL demonstrated accelerated aggregation response within 10 hours in contrast to WT ME-Macs, suggesting increased aggregation activity in 3KL ME-Macs (Fig. 1n,o). No activity was observed in isolated enteric neurons from either 3-month 3KL or WT mice, despite the expression of total αS in enteric neurons but absence in ME-Macs (Fig. 1n–p and Extended Data Fig. 2l). The presence of αS aggregates in 3KL ME-Macs was further confirmed using the amyloid-binding dye Amytracker in isolated ME-Macs by flow cytometry (Extended Data Fig. 2m). In line with SAA data, we observed increased Amytracker signal in ME-Macs of 3-month 3KL versus WT mice but did not find positive signal in lamina propria Macs (Extended Data Fig. 2m,n). Together, these results indicate ME-Macs as potential modulators of αS amyloid aggregates in the ENS.

To further explore the gut–brain axis in synucleinopathy, we directly injected human PD brain-extracted αS fibrils (PD) versus identically extracted human neurological healthy control (NHC) brain preparations into ME of *Snca*$^{WT/GFP}$ knock-in mice[3,4,23] (Extended Data Fig. 3a–e and Supplementary Table 1b). We used a purification protocol specifically designed to select for amyloid and other highly insoluble proteins[24]. The brain-extracted αS fibrils are hereafter designated as PD-αS and NHC-αS, respectively. Duodenal injection of PD-αS but not NHC-αS in ME increased endogenous αS expression in myenteric ganglia (Fig. 2a,b). We observed significant upregulation of s129p$^+$ αS immunoreactivity at 1 month and 3 months postinjection, predominantly around neuronal cell bodies and to a lesser extent, in extraganglionic neurons, similar to 3-month 3KL (Fig. 2a–d). Prolonged total gut transit time was found post-PD-αS injection (Fig. 2e). Significant increase of s129p$^+$ αS inclusions was observed at 3 months post-PD-αS injection in the brainstem (Fig. 2f,g). Further, an increased fraction of s129p$^+$ αS in dopaminergic neurons of the substantia nigra pars compacta (SNpc) was observed, suggesting a potential route for pathological spread from the ENS to the CNS (Fig. 2h,i). We observed a selective loss of dopaminergic neurons in the SNpc at 3 months post-PD-αS versus

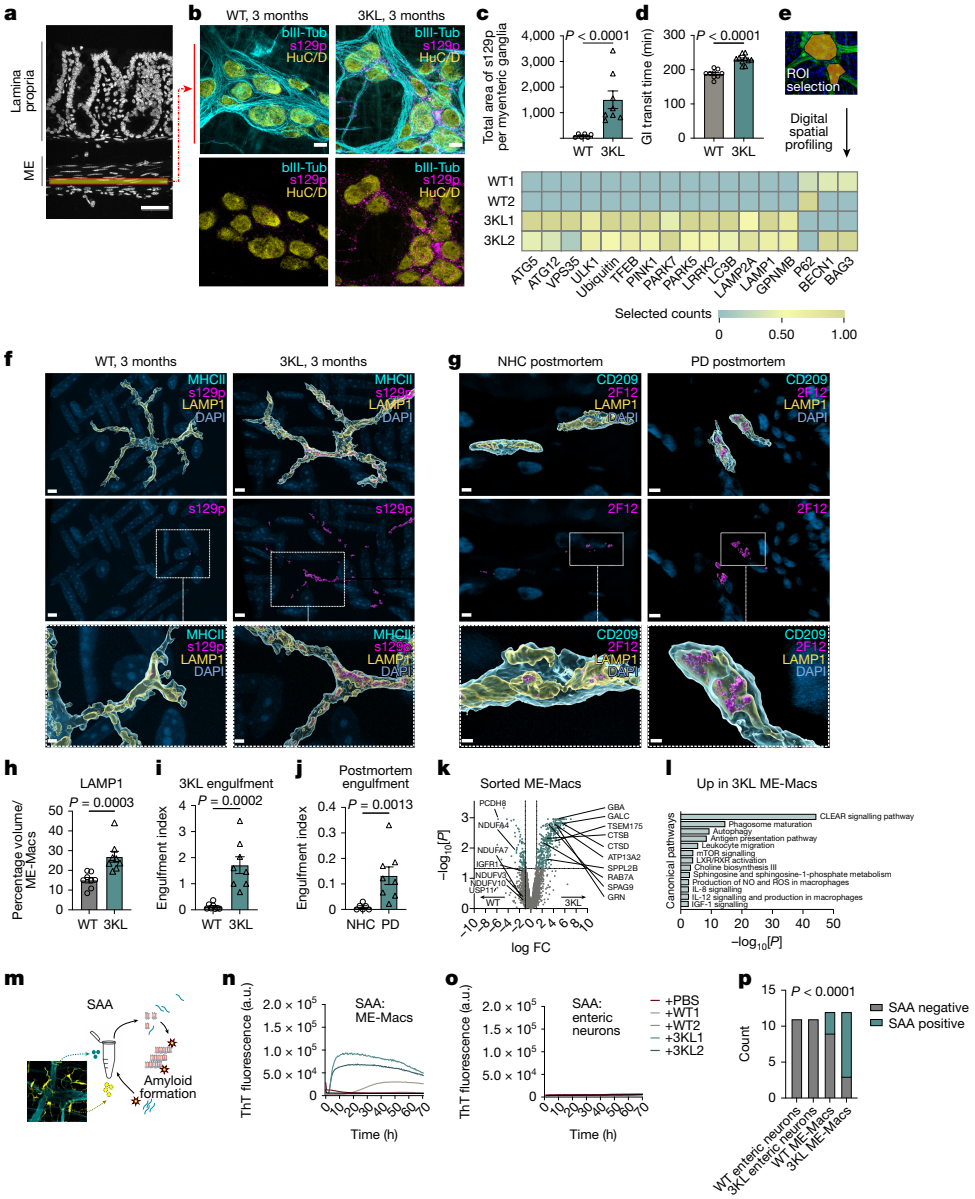

Fig. 1 | ME-Macs engulf and modify αS pathology in 3KL αS transgenic mice. **a**, Schematic of gut cross-section. **b**, Confocal image of duodenal myenteric plexus of 3-month WT versus 3KL. **c**, Quantification of s129p$^+$ αS pathology: $n = 6$–8 mice; 1 datapoint, average of 1 mouse; 3–10 ROIs per mouse. Three experiments, data analysed using an unpaired *t*-test. **d**, Whole gastrointestinal transit time in 3-month WT versus 3KL, $n = 9$–10. Two experiments, unpaired *t*-test. **e**, Hierarchically clustered heatmap of ROI-specific nCounter digital counts across PD-relevant protein targets in duodenal myenteric plexus of 3-month WT versus 3KL, $n = 2$, 2–3 ROIs per mouse. **f**–**j**, Confocal images of engulfed αS by murine MHCII$^+$ duodenal (**f**) and human CD209$^+$ jejunal (**g**) ME-Macs, quantified murine LAMP1 lysosomal volume (**h**) and engulfment of s129p in murine (**i**) and αS (2F12) in human (**j**) LAMP1$^+$ lysosomes. $n = 8$ mice per genotype (**h**,**i**) and $n = 6$ NHC and 8 PD postmortem samples (**j**). Two experiments, Mann–Whitney test (**h**–**j**). **k**, Volcano plot showing differentially expressed proteins in sorted ME-Macs of 3-month WT versus 3KL. $n = 2$ per genotype, with 3 mice pooled per biological unit. **l**, Biological processes enriched in 3-month 3KL ME-Macs, one-sided hypergeometric test. **m**, Schematic of SAA on sorted duodenal ME-Macs versus enteric neurons. **n**,**o**, αS aggregation kinetics through SAA in duodenal enteric neurons (**n**) and ME-Macs (**o**). **p**, SAA-positive versus negative count in different cell lysates. A sample was counted positive if aggregation onset (lag time) was at least 2 h shorter than negative control (PBS). $n = 11$ (enteric neurons), $n = 12$ (ME-Macs). Six experiments, Fisher's exact test. Data are mean ± s.e.m. (error bars). FC, fold change; GI, gastrointestinal; NO, nitric oxide; ROS, reactive oxygen species; ThT, thioflavin T. Scale bars, 50 µm (**a**); 10 µm (**b**); 5 µm (**f**–**j**), insets 2 µm (**f**–**j**).

NHC-αS injections (Fig. 2j,k and Extended Data Fig. 3f). By contrast, no dopaminergic neuronal loss was observed in the ventral tegmental area (VTA), consistent with the region-specific dopaminergic neuronal vulnerability in patients with PD[25] (Fig. 2k). We then investigated whether ME-Macs engulfed s129p$^+$ αS in response to PD-αS injections and observed a roughly 13-fold increase in lysosomal s129p$^+$ αS in ME-Macs in PD-αS-injected animals compared with NHC-αS-injected controls at 1 month postinjection (Extended Data Fig. 3g–i). However, we found no overt production of inflammatory cytokines in the ME, suggesting the absence of local inflammation in the ME induced by αS injections (Extended Data Fig. 3j). These data indicate that body-first αS pathology, triggered by PD-αS injection into the ME, propagates from the ENS to the CNS, leading to region-specific dopaminergic neuron loss.

A gut-to-brain T cell axis in PD

Recent studies reported increased CD3$^+$ T cell numbers in intestinal biopsies of constipated patients with PD versus healthy control

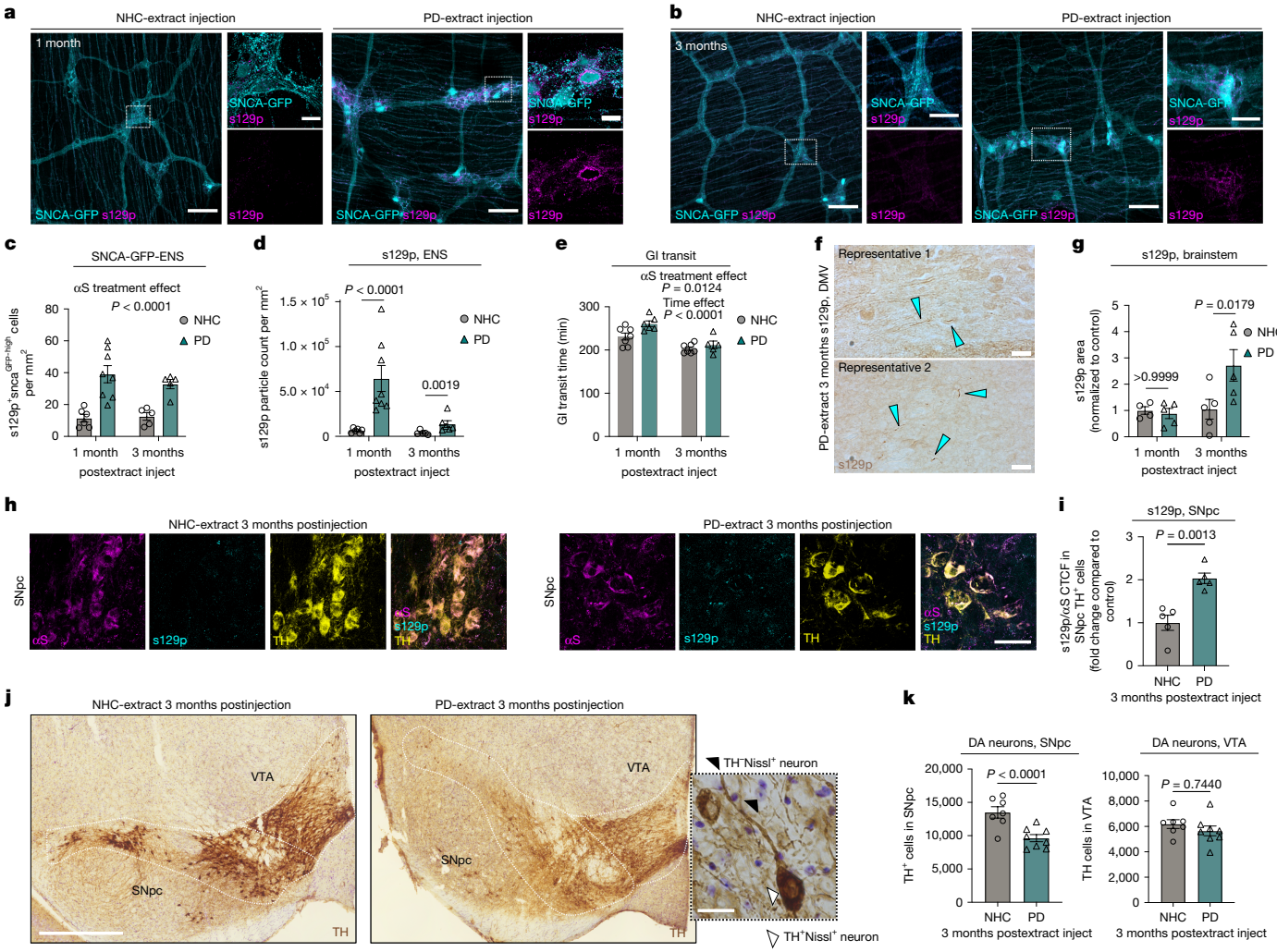

Fig. 2 | ME injection of PD-extracts triggers αS pathology along the gut–brain axis. a,**b**, αS s129p$^+$ pathology in duodenal myenteric plexus at 1 month (**a**) and 3 months (**b**) post-NHC-αS versus PD-αS injection. **c**, Quantification of αS-GFP^{high} cells per mm^2 at 1 month and 3 months postinjection. $n = 6$ for αS-NHC, 1 month; $n = 8$ for αS-PD, 1 month; $n = 5$ for αS-NHC and αS-PD, 3 months. Two experiments. **d**, Quantification of αS s129p$^+$ pathology at 1 month and 3 months postinjection. One datapoint, average of 1 mouse, 5–9 ROIs per mouse. $n = 6$ mice for αS-NHC, 1 month; $n = 8$ for αS-PD, 1 month; $n = 5$ mice for αS-NHC and $n = 6$ mice for αS-PD, 3 months. Two experiments. **e**, Gastrointestinal transit time at 1 month and 3 months postinjection. $n = 7$ mice for αS-NHC, $n = 6$ mice for αS-PD, 1 month; $n = 7$ mice for αS-NHC, $n = 5$ mice for αS-PD, 3 months. Two experiments, data analysed using two-way ANOVA (**c**–**e**) with Bonferroni's multiple-comparison test (**d**). **f**, Widefield images of s129p$^+$ αS pathology in brainstem at 3 months postinjection, blue arrows highlight αS inclusions. **g**, Quantification of s129p$^+$ αS pathology in brainstem at 1 month and 3 months postinjection, $n = 4$ mice for αS-NHC, 1 month and $n = 5$ mice for αS-NHC, 3 months; αS-PD, 1 month and 3 months. Two experiments, two-way ANOVA with Bonferroni's multiple-comparison test. **h**, αS s129p$^+$ pathology in SNpc at 3 months post-NHC versus PD-extract injection. **i**, CTCF of s129p αS normalized to total αS, $n = 5$ mice per group. Two experiments, unpaired *t*-test. **j**, TH$^+$ immunostainings in SNpc and VTA using DAB, 3 months post-treatment. brightfield micrograph of dopaminergic neurons in the SNpc. **k**, Unbiased stereological quantification of TH$^+$ cells in SNpc and VTA, $n = 7$ mice for αS-NHC, SNpc and VTA, $n = 8$ mice for αS-PD, SNpc and VTA. Three experiments, mixed-effect model with multivariate *t*-distribution posthoc test. Data are mean ± s.e.m. (error bars). Scale bars, 100 µm (**a**,**b**), insets 20 µm (**a**,**b**,**j**); 20 µm (**f**,**j**); 50 µm (**h**); 500 µm (**j**). DA, dopaminergic.

participants and in PD mouse models that show prodromal constipation[26,27]. Further, increased numbers of T cells are found in the plasma and brain of patients with PD, but with unknown origin[5,6,28]. In addition to endolysosomal pathways, proteomic signature analysis on isolated ME-Macs from 3KL mice revealed upregulation of antigen presentation and leukocyte migration pathways (Fig. 1l and Extended Data Fig. 2j). MHCII, which enables antigen presentation to T cell receptors (TCRs), was found increased on ME-Macs (Extended Data Fig. 2g). These data suggest a potential engagement of adaptive immune cells after ME-Mac uptake of pathological αS. Hence, we asked whether CD3$^+$ T cells are expanded in the ENS in response to αS pathology. IHC on myenteric plexus of 3-month 3KL versus WT mice showed increased numbers of CD3$^+$ T cells in 3-month 3KL mice (Fig. 3a–c). Of note, T cells were primarily found adjacent to myenteric ganglia (Fig. 3a,b). Flow cytometry confirmed increased proportions of CD3$^+$ T cells among total CD45$^+$ cells isolated from 3-month ME, with an increased CD4$^+$ to CD8$^+$ ratio in 3-month 3KL mice (Fig. 3d–e and Extended Data Fig. 4a). This is in line with previous studies demonstrating a predominant role for CD4$^+$ T cell responses in αS pathology in mice and human PD[29]. Of note, T cell expansion was less obvious in the lamina propria (Extended Data Fig. 4b). Further, the increased proportions of CD3$^+$CD4$^+$ T cells in myenteric plexus were also observed in the ME PD-αS versus NHC-αS injection model, as demonstrated by IHC and flow cytometry (Fig. 3f–j). We assessed T cells in the ME of human patients with PD by performing IHC on postmortem jejunum and observed similar expansion of CD4$^+$ T cells in myenteric plexus of PD versus NHC patients (Fig. 3k,l and Supplementary Table 1a).

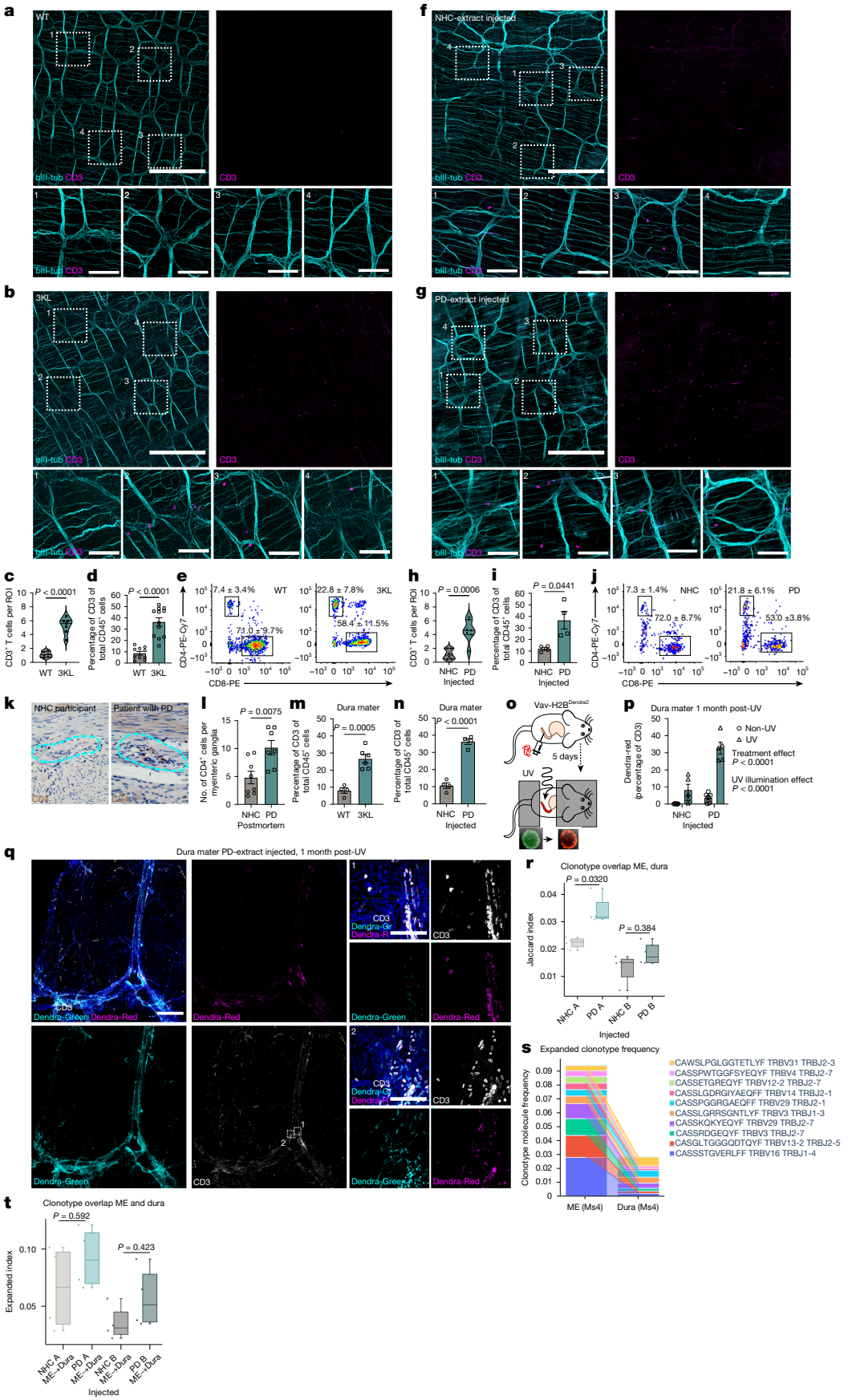

Fig. 3 | See next page for caption.

Fig. 3 | T cells expand in the ENS and travel to the CNS in synucleinopathy. **a**,**b**, $CD3^+$ T cells in duodenal myenteric plexus of 3-month WT (**a**) versus 3KL (**b**) mice. Inset, ROI for counting. **c**,**d**, $CD3^+$ T cells in 3KL myenteric plexus per ROI, quantified by IHC (**c**) and FACS (percentage of ME $CD45^+$ cells) (**d**). $n = 6$ mice (WT), $n = 7$ mice (3KL) (**c**) or $n = 10$ mice (WT), $n = 12$ mice (3KL) (**d**). Two (**c**) and four (**d**) experiments, data analysed using an unpaired *t*-test with Welch's correction (**c**,**d**). **e**, FACS plots of $CD4^+CD8^+$ ME T cells in 3-month WT versus 3KL. **f**,**g**, $CD3^+$ T cells in duodenal myenteric plexus post-NHC-αS (**f**) versus PD-αS (**g**). Inset, ROI used for counting. **h**,**i**, $CD3^+$ T cells in 3KL myenteric plexus per ROI, quantified by IHC (**h**) and FACS (percentage of ME $CD45^+$ cells) (**i**). $n = 6$–7 (**h**) or $n = 4$ (**i**) mice per genotype. Two experiments, unpaired *i*-test (**h**) with Welch's correction (**i**). **j**, FACS plots of $CD4^+CD8^+$ ME T cells post-NHC-αS versus PD-αS. **k**,**l**, DAB staining of ME $CD4^+$ T cells in jejunum of PD versus NHC patients (**k**) and quantification (**l**). $n = 7$–8 per disease status. Two experiments, unpaired *t*-test. **m**,**n**, $CD3^+$ T cells in dura mater of 3-month 3KL versus WT (**m**) or 1 month post-NHC-αS versus PD-αS (**n**) quantified by FACS (percentage of total dura mater $CD45^+$ cells), $n = 4$ mice (WT), $n = 6$ mice (3KL) (**m**) or $n = 4$ mice per treatment (**n**). Two experiments, unpaired *t*-test. **o**, Schematic of T cell photoconversion in VHD mice, 5 days post-NHC-αS versus PD-αS. **p**, Dendra-red $CD3^+$ T cells in dura mater at 1 month post-NHC-αS versus PD-αS injection and UV versus non-UV photoconversion, $n = 5$–6 per genotype. Note minor leakage in the absence of UV illumination. Four experiments, two-way ANOVA. **q**, Dendra-red versus dendra-green $CD3^+$ T cells in dura mater, 1 month post-PD-αS injection and UV illumination in ME. Representative of five mice (overview). **r**, Boxplot quantifying clonotype overlap between ME and dura mater through the Jaccard index (Methods, equation (1)) of NHC-αS- and PD-αS-injected groups for α (A) and β (B) TCR chains. Bonferroni-adjusted unpaired *t*-test with Welch's correction. Data are shown as boxplots: the median is the central line; hinges indicate the first and third quartiles; whiskers extend to the most extreme values within the 1.5× interquartile range and points beyond the whiskers are plotted as individual outliers. **s**, Alluvial plots of the top ten most frequent T cell clone β chains in ME and dura mater of one representative mouse from PD-αS. **t**, Boxplot quantifying the clonotype overlap between the ME and dura mater through the expanded index (Methods, equation (3)) of NHC-αS- and PD-αS-injected groups for α (A) and β (B) TCR chains. Bonferroni-adjusted unpaired *t*-test with Welch's correction. Data are mean ± s.e.m. (error bars). Scale bars, 500 µm (**a**,**b**,**f**,**g**); 50 µm (**k**); 1 mm (**q**); insets 50 µm (**a**,**b**,**f**,**g**); 25 µm (**q**).

Together, these results show that $CD4^+CD3^+$ T cells regionally infiltrate the ME of PD mouse models and patient tissues.

Next, we asked whether T cells could distribute from the ENS to CNS according to the spatiotemporal distribution of αS pathology. Many studies have demonstrated infiltration of $CD3^+$ T cells into the CNS in preclinical models of PD and postmortem tissue, but the peripheral site of origin remained elusive[29]. We first evaluated $CD3^+$ T cell numbers in the dura mater, a peripheral-brain interface in the leptomeninges that allows access of T cells into the brain parenchyma[30]. We found that $CD3^+$ T cells were significantly elevated in the dura mater of PD-αS-injected and 3KL mice (Fig. 3m,n and Extended Data Fig. 4c). To test whether dural $CD3^+$ T cells could originate from the intestine, we injected PD-αS versus NHC-αS in Vav-H2B-Dendra2 (VHD) mice expressing H2B-dendra2 protein under control of haematopoietic *Vav*, allowing tracking of dendra2 photoconverted immune cells[31] (Fig. 3o). Ultraviolet (UV) exposure of ME from VHD mice caused irreversible photoconversion in ME $CD3^+$ T cells, $Ly6G^+$ neutrophils and $CD11b^+$ myeloid cells at 24 hours post-UV illumination (Extended Data Fig. 4d–f). UV exposure did not label circulating $CD3^+$ T cells in the blood at 1 hour post-UV (Extended Data Fig. 4g). We characterized photoconversion kinetics in T cells at 3 days, 7 days and 31 days post-UV illumination and PD-αS injection and detected circulating dendra-red^+ T cells in the blood between 3 days and 7 days postillumination but declining at 31 days, whereas photoconverted T cells were increasingly observed in the dura mater between 7 days and 31 days postillumination (Fig. 3p and Extended Data Fig. 4h,i). Notably, roughly 2% of lymphocytes are dendra-negative, probably reflecting incomplete *Vav* promoter efficiency. A small percentage of T cell photoconversion was detected in the lamina propria, highlighting their potential contribution to the dura mater T cell pool (Extended Data Fig. 4h). Minor dendra-red cell presence was observed in dura mater of control illuminated αS-treated mice, indicating slight leakiness of the model (Fig. 3p and Extended Data Fig. 4j). In addition, photoconverted $CD64^+$ cells were detected in the dura mater of PD-αS-injected mice, suggesting migration of myeloid cells from the duodenum (Extended Data Fig. 4k). Whole-mount imaging of the dura mater of PD-αS-injected mice confirmed presence of dendra-red $CD3^+$ T cells (Fig. 3q and Extended Data Fig. 4l,m). Together, these data indicate expansion of ME T cells in the context of αS pathology, and that a proportion of intestinal T cells migrates to the dura mater.

To confirm that T cells in the ME and brain were clonally related, and to measure clonal expansion, we performed TCR sequencing on ME and dura mater, striatum and hippocampus samples collected 10 days post-NHC-αS and PD-αS injection. The number of TCRs recovered from striatum and hippocampus at this early time point was very small, so we focused analysis on the dura mater. The diversity (inverse Simpson) of the repertoires showed a trending decrease following PD-αS injection, suggestive of antigen-driven clonal expansion (Extended Data Fig. 5a). In agreement with the increased dendra-red $CD3^+$ T cells observed in PD-αS-injected mice, there was an increase in TCR sequence sharing between ME T cells and dura mater T cells following injection of PD-αS (Fig. 3r). The degree of overlap was greater for TCRα than for TCRβ, reflecting the higher diversity of the TCRβ[32]. Many of the TCRs shared between ME and dura mater showed significant clonal expansion, consistent with previous antigen recognition (Fig. 3s and Extended Data Fig. 5b,c). A trend for increased sharing of expanded ME T cells to the dura mater in PD-αS-injected versus NHC-αS-injected mice was observed (Fig. 3t). Taken together, these data indicate expansion of ME T cells in the context of αS pathology, and that a proportion of expanded intestinal T cells migrates to the dura mater, potentially mediated by PD-αS.

ME-Mac–T cell crosstalk through TGFβ1

We next explored whether the observed T cell expansion involved crosstalk with ME-Macs that are reactive to αS pathology. IHC and 3D reconstruction revealed close proximity between ME-Macs and T cells in the myenteric plexus of 3-month 3KL mice and patients with PD (Fig. 4a). To elucidate transcriptional changes in ME-Macs and T cells on αS pathology and cellular interactions among them, we performed single-cell RNA sequencing (scRNA-seq) using the 10X Genomics platform on fluorescence-activated cell-sorted duodenal ME $CD3^+$ cells and ME-Macs of 4-month 3KL and WT mice, a time point chosen to capture profiles after initial T cell expansion (Fig. 4b and Extended Data Fig. 6a,b). After quality control, we ran unsupervised clustering on 2,748 cells and identified clusters of ME-Macs (*Adgre1* and *Csf1r*) and T cells (*Cd3* and *Cd8a*) (Fig. 4b and Extended Data Fig. 6b–d). We found three transcriptionally distinct ME-Mac subclusters based on *Cd163* and *Ccr2* expression, resembling previously described tissue-resident macrophage subtypes associated with blood vessels (*Lyz2*, *Mrc1*, *Pf4*) and neurons (*H2-Dma*, *H2-Aa*, *Cd74*)[33] (Fig. 4b, Extended Data Fig. 6d and Supplementary Table 2). *Cd163*$^+$ ME-Macs expressed transcripts involved in leukocyte migration and chemotaxis, whereas *Ccr2*$^+$ ME-Macs were enriched in transcripts related to antigen processing (Extended Data Fig. 6e). The third cluster, hereafter referred to as *Cd163*$^-$*Ccr2*$^-$ ME-Macs, demonstrated upregulation of genes related to leukocyte migration and cytokine signalling. We validated the presence of $CD163^+$, $CCR2^+$ and $CD163^-CCR2^-$ $IBA1^+$ ME-Macs using flow cytometry and IHC (Fig. 4c,d and Extended Data Fig. 6f–l). Flow cytometry revealed no differences in absolute subcluster numbers between WT

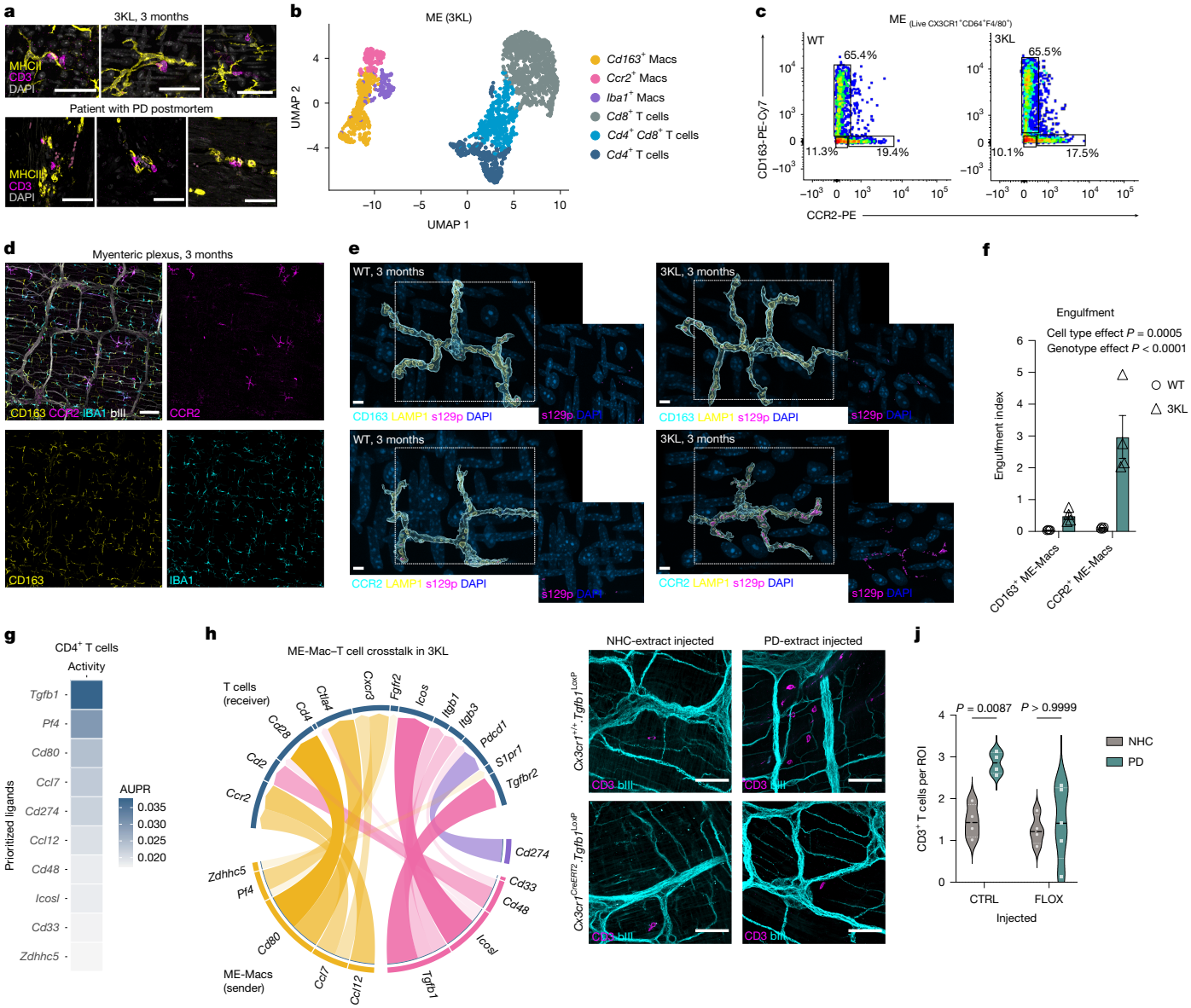

Fig. 4 | ME-Macs and T cells interact by means of TGFβ1 in body-first PD models. a, Confocal images of ME-Macs and ME T cells in 3-month 3KL and PD postmortem ME. Representative of more than four experiments. **b**, Uniform manifold approximation and projection (UMAP) of unsupervised clustering of ME-Macs and T cells from ME assigned into colour-coded subclusters. scRNA-seq data obtained from fluorescence-activated cell-sorted ME-Macs and ME CD3$^+$ cells of 4-month 3KL and WT subjected to 10X Genomics scRNA-seq (n = 2,748 cells). Four biologically independent samples were used, and samples were sequenced in n = 2 batches from WT versus 3KL. One sample represents ME pooled from 4 mice. **c**,**d**, FACS plots (**c**) and confocal images (**d**) demonstrating CD163$^+$, CCR2$^+$ and CD163$^-$CCR2$^-$ duodenal ME-Macs in 3-month WT versus 3KL (**c**) or 3KL (**d**). Data representative of three experiments. **e**,**f**, Confocal images (**e**) of s129p engulfment by CD163$^+$ and CCR2$^+$ duodenal ME-Macs in 3-month WT versus 3KL and quantification (**f**), n = 4 per genotype. One experiment, two-way repeated measures ANOVA. **g**, Heatmap showing top ligands expressed in ME-Macs ranked on the basis of area under the precision–recall curve (AUPRC) with 3KL T cells as receivers. **h**, Circos plot showing ligand–receptor pairs between ME-Macs and T cells in 4-month 3KL. Bottom, top eight ligands expressed by 3KL ME-Macs. Top, differentially expressed receptors in 3KL versus WT T cells. **i**,**j**, Confocal images (**i**) of duodenal ME T cells in *Cx3cr1*$^{+/+}$.*Tgfb1*^{LoxP} versus *Cx3cr1*^{CreERT2}.*Tgfb1*^{LoxP} at 10 days post-NHC-αS versus PD-αS injection and quantification (**j**), n = 4 mice (CTRL, NHC-αS and PD-αS; FLOX, NHC-αS) and n = 5 mice (FLOX, PD-αS). Two experiments, two-way ANOVA, Bonferroni's multiple-comparison test. Data are mean ± s.e.m. (error bars). Scale bars, 30 µm (3KL, **a**); 50 µm (PD, **a**); 100 µm (**d**); 50 µm (**i**). AUPRC, area under the precision–recall curve.

and 3KL mice at 3–4 months (Extended Data Fig. 6h). However, CCR2$^+$ ME-Macs were generally significantly fewer in 3KL mice, reaching significance at 6 months. IHC showed altered proportions of CD163$^+$ and CD163$^-$CCR2$^-$ ME-Macs in 3-month-old 3KL mice but no differences in PD-αS- versus NHC-αS-injected animals (Extended Data Fig. 6i–l).

We next examined whether CD163$^+$ and CCR2$^+$ ME-Macs showed increased capacity to engulf s129p$^+$ αS in PD models. In 3-month 3KL mice, both populations showed increased αS engulfment compared with WT (Fig. 4e,f). Similarly, in the injection model, αS engulfment was increased in both ME-Mac subsets 1 month post-PD-αS injection (Extended Data Fig. 6m,n). These findings indicate that ME-Macs show an enhanced ability to internalize αS in the context of PD-associated pathology.

To evaluate how ME-Macs could modulate T cells transcriptionally, we used NicheNet on our scRNA-seq data to predict ligand–receptor interactions between ME-Macs and T cells[34] (Fig. 4g,h and Extended Data Fig. 7a,b). We focused on disease-specific interactions under 3KL conditions, selecting receptor transcripts that

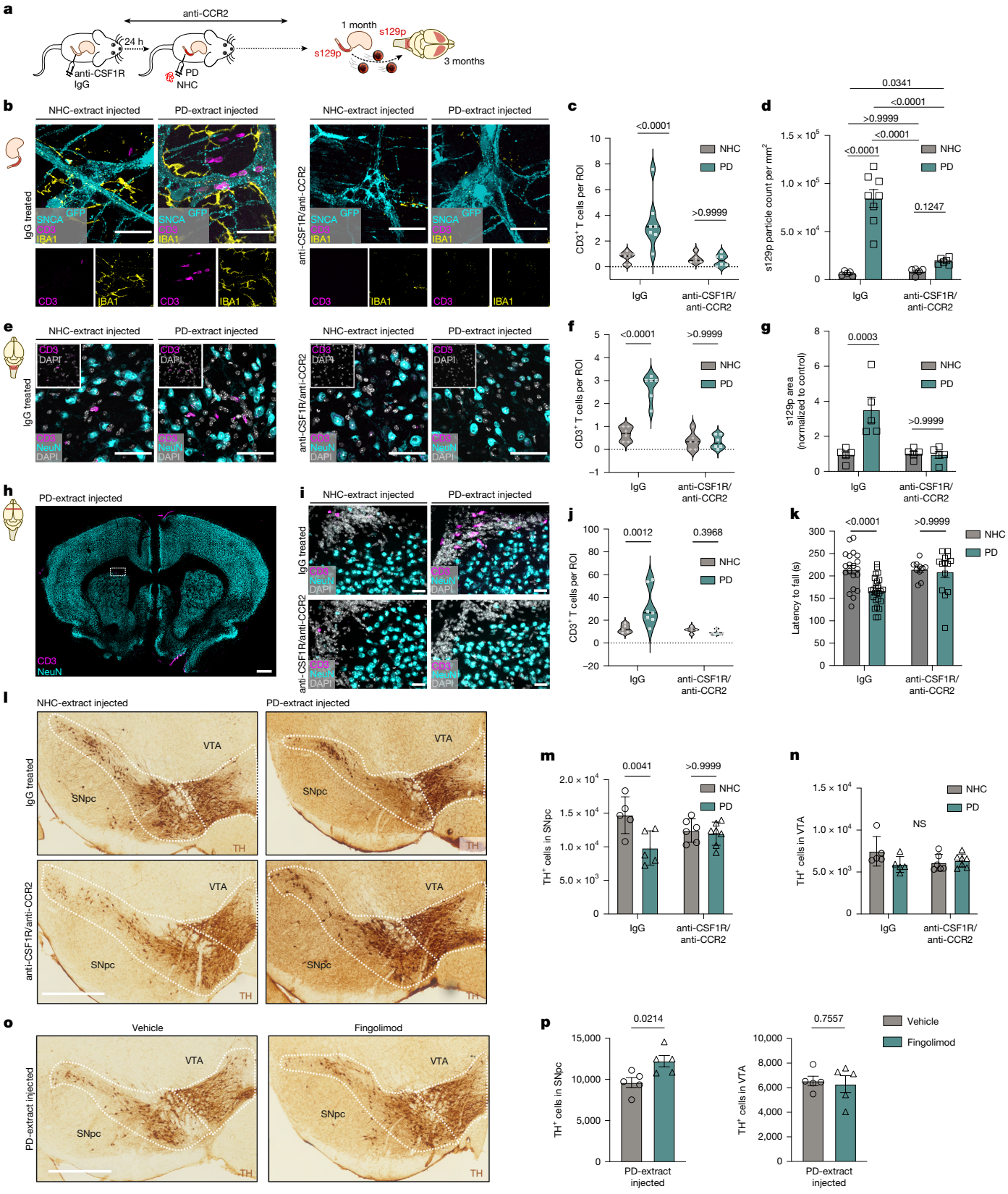

Fig. 5 | See next page for caption.

were differentially expressed in T cells and corresponding ligands expressed by 3KL ME-Macs. The ligand with the highest regulatory potential was *Tgfb1*, which was predominantly expressed by CCR2$^+$ and CD163$^+$ ME-Macs, whereas its canonical receptor *Tgbr2* was expressed by ME T cells[35] (Fig. 4g,h and Extended Data Fig. 7c). We next investigated the role of TGFβ1 in ME-Mac–T cell crosstalk in the context of αS pathology. Tamoxifen-treated *Cx3cr1*^{CreERT2}.*Tgfb1*^{LoxP} mice were injected with NHC-αS or PD-αS injections 4 months later, when *Tgfb1*

Fig. 5 | Directed depletion of ME-Macs ameliorates αS pathology, prevents T cell expansion and improves motor behaviour. a, Schematic of directed ME-Mac depletion using anti-CSF1R/anti-CCR2 treatment. **b**, Confocal images of $CD3^+$ T cells, $IBA1^+$ ME-Macs and αS in duodenal myenteric plexus of NHC-αS versus PD-αS, anti-CSF1R/anti-CCR2 versus IgG treatment, 1 month postinjection. **c**,**d**, Quantification of $CD3^+$ T cells (**c**) and $s129p^+$ αS pathology (**d**) in myenteric plexus at 1 month post-NHC-αS versus PD-αS, anti-CSF1R/anti-CCR2 versus IgG treatment. $n = 5$ mice for NHC-αS, anti-CSF1R/anti-CCR2; $n = 6$ mice for PD-αS, anti-CSF1R/anti-CCR2; $n = 7$ mice for NHC-αS and PD-αS, IgG (**c**) or $n = 5$ mice for NHC-αS, IgG and anti-CSF1R/anti-CCR2; $n = 8$ mice for PD-αS, IgG and $n = 6$ mice for PD-αS, anti-CSF1R/anti-CCR2 (**d**). Two experiments, data analysed using two-way ANOVA, Bonferroni's multiple-comparison test. **e**,**f**, Confocal images of $CD3^+$ T cells in brainstem at 3 months post-treatment (**e**) and quantification (**f**), $n = 6$ mice. Two experiments, two-way ANOVA, Bonferroni's multiple-comparison test. **g**, $S129p^+$ αS pathology in brainstem at 3 months post-treatment, $n = 5$ mice. Two experiments, two-way ANOVA, Bonferroni's multiple-comparison test. **h**–**j**, Confocal images of $CD3^+$ T cells in forebrain (**h**) (inset, dorsal border of the striatum) at 3 months post-treatment (**i**) and quantification (**j**), $n = 5$ mice for NHC-αS, IgG and anti-CSF1R/anti-CCR2 and $n = 7$ mice for PD-αS, IgG and anti-CSF1R/anti-CCR2. Two experiments, two-way ANOVA, Bonferroni's multiple-comparison test. **k**, Latency to fall on an accelerating rotarod at 3 months post-treatment, $n = 20$ mice for NHC-αS, IgG; $n = 27$ mice for PD-αS, IgG; $n = 10$ mice for NHC-αS, anti-CSF1R/anti-CCR2; $n = 14$ mice for PD-αS, anti-CSF1R/anti-CCR2 over seven experiments, two-way ANOVA, Bonferroni's multiple-comparison test. **l**, TH^+ immunostainings in SNpc and VTA of ventral midbrain sections using DAB, 3 months post-treatment. **m**,**n**, Unbiased stereological quantification of TH^+ cells in SNpc (**m**) and VTA (**n**), $n = 5$ mice for NHC-αS and PD-αS, IgG; $n = 6$ mice for NHC-αS, anti-CSF1R/anti-CCR2; $n = 7$ mice for PD-αS, anti-CSF1R/anti-CCR2 over three experiments. Two-way ANOVA, Bonferroni's multiple-comparison test (**m**). NS, not significant. **o**,**p**, TH^+ immunostainings using DAB, 3 months post-PD and fingolimod treatment (**o**) and unbiased stereological quantification (**p**), $n = 5$ mice. One experiment, unpaired *t*-test. Data are mean ± s.e.m. (error bars). Scale bars, 50 μm (**b**,**h**,**e**,**f**,**i**); 500 μm (**l**,**o**).

deletion is retained only in self-maintaining macrophages[8] (Extended Data Fig. 7d–f). Notably, PD-αS failed to induce T cell expansion in *Cx3cr1*^{CreERT2}.*Tgfb1*^{LoxP} mice, unlike in *Cx3cr1*$^{+/+}$.*Tgfb1*^{LoxP} and NHC-αS controls (Fig. 4i,j). Whereas absolute $IBA1^+$ ME-Mac counts, $CD163^+$ or $CCR2^+$ proportions, and lysosomal numbers remained unchanged, a proportional increase in $CD163^-CCR2^-$ $IBA1^+$ ME-Macs was observed in both genotypes (Extended Data Fig. 7g–j). T cell numbers in the lamina propria were unaffected[12] (Extended Data Fig. 7k,l).

ME-Mac targeting reduces PD pathology

We next asked whether ME-Macs could directly modulate the expansion of T cells to the brain in response to αS pathology. We aimed to deplete ME-Macs by injecting anti-CSF1R antibody (AFS98) into duodenal ME at 24 hours before αS treatment[9] (Fig. 5a and Extended Data Fig. 8a). We combined anti-CSF1R with anti-CCR2 antibody (MC21) treatment to circumvent immediate monocyte replenishment and to extend the depletion of ME-Macs in the myenteric plexus[8]. Of note, this approach resulted in minor depletion of other immune cells, including reduced numbers of ME monocytes, ME eosinophils and lamina propria monocytes at 5 days post-treatment, as well as decreased circulating neutrophils at 5 days and circulating monocytes at 24 hours and 5 days post-treatment (Extended Data Fig. 8b,c). Microglia and border-associated macrophages were not affected by this treatment (Extended Data Fig. 8d). T cell expansion on PD-αS versus NHC-αS injection was abolished in the myenteric plexus at 1 month post-anti-CSF1R/anti-CCR2 versus IgG treatment, suggesting that ME-Macs are potentially involved in the T cell expansion in αS models (Fig. 5b,c). Further, we observed amelioration of $s129p^+$ αS pathology at 1 month post-PD-αS injection in mice pretreated with anti-CSF1R/anti-CCR2 compared with IgG, suggesting the contribution of ME-Macs in the progression of αS pathology along the ENS (Fig. 5d). Given that fractions of T cells could travel from the ME to the dura mater on PD-αS treatment, we next asked whether ME-anti-CSF1R/anti-CCR2 could alter T cell expansion in the CNS. We focused on the brainstem and striatum that sequentially undergo αS pathology per Braak staging[11]. We found a significant increase in $CD3^+$ cell number in the brainstem of 3 months post-PD-αS versus NHC-αS injection; however, this increase was abolished when mice were pretreated with anti-CSF1R/anti-CCR2 (Fig. 5e,f). In addition, $s129p^+$ αS pathology was ameliorated in the brainstem, suggesting that ME-Macs contribute to the progression of αS pathology from ENS to CNS (Fig. 5g). Next, we focused on the striatum, a region highly innervated by dopaminergic neurons, the degeneration of which is suggested to underlie motor symptoms in PD[36]. We observed increased $CD3^+$ cell numbers in the dorsal border of the striatum adjacent to the corpus callosum at 3 months post-PD-αS versus NHC-αS injection, whereas mice pretreated with anti-CSF1R/anti-CCR2 failed to initiate $CD3^+$ cellular expansion (Fig. 5h–j). We next investigated whether the directed depletion of ME-Macs could ameliorate motor behaviour on αS pathology. Animals injected with PD-αS versus NHC-αS showed impaired performance on a slowly accelerating rotarod at 3 months postinjection; however, this deficit was reversed in mice pretreated with anti-CSF1R/anti-CCR2 (Fig. 5k). Consistent with this, pretreatment with anti-CSF1R/anti-CCR2 also mitigated the region-specific loss of dopaminergic neurons in the SNpc induced by PD-αS (Fig. 5l–n). Finally, treatment with fingolimod, which downregulates the sphingosine-1 phosphate receptor and prevents lymphocyte egress from lymph nodes[37], mitigated PD-αS-induced dopaminergic neurodegeneration in the SNpc specifically, suggesting a role for T cell trafficking in αS-mediated neurodegeneration (Fig. 5o,p). Together, our data suggest that ME-Macs modulate T cell response along the gut–brain axis in the context of αS pathology. Prolonged anti-CSF1R/anti-CCR2 treatment of the ME prevents T cell expansion and ameliorates $s129p^+$ αS pathology in the ENS and CNS, while preventing T cell egression into the bloodstream reduced neurodegeneration. Together, our findings suggest that manipulation of the gut–immune–brain axis could modulate motor phenotype and ameliorate neurodegeneration in PD.

Discussion

Our work suggests that ME-Macs contribute to the initiation and spreading of pathological αS along the gut–brain axis in PD. We found that ME-Macs modulate $s129p^+$ αS pathology on engulfment and facilitate T cell expansion from ENS to CNS. Consistently, directed ME-Mac depletion ameliorates the progression of αS pathology towards the brainstem and motor dysfunction. These results indicate ME-Macs as early cellular mediators of αS pathology along the gut–brain axis, presenting cellular mechanisms that may underlie body-first PD.

In contrast to familial PD, sporadic PD is probably the result of interacting genetic and environmental factors that influence the region-specific onset and cell-to-cell progression of αS[38,39]. In parallel, the Braak staging system implies that in body-first patients with PD, initial deposition of pathological αS occurs in the ENS before it migrates and distributes to the CNS[11]. In the brain, αS pathology further spreads in a rostro-caudal manner from inferior brain regions to midbrain regions where it perturbs normal motor functions. We observed early αS pathology in the ENS of 3KL αS transgenic mice, coinciding with increased gastrointestinal transit time. Further, we found evidence that PD-αS directly injected into the ME could propagate to the brain and cause progressive neurodegeneration and motor impairments in mice, highlighting its significance as a model for studying αS propagation along the gut–brain axis. Notably, we observed region-specific $s129p^+$ αS deposition in the ENS correlated with the upregulation of PINK1, LRRK2 and VPS35, associated with late-onset PD and involved in

lysosomal biology[40,41]. This is in line with previous work demonstrating endolysosomal dysfunction in mice injected with αS fibrils into the ME, probably reflecting the continuing clearance of αS aggregates by macrophages and underscoring the key role of non-neuronal cells in impaired αS degradation[3]. The observed increase in total gut transit time in these mice suggests that ENS integrity could be directly affected by phosphorylated αS. The slow-transit phenotype was ameliorated by 3 months postinjection, suggesting that intestinal immune responses can resolve with time.

Our study highlights a central role for ME-Macs in the development of αS pathology along the gut–brain axis. ME-Macs are self-maintaining macrophages that have a crucial role in ENS homeostasis and function[8,9]. In PD mouse models, we found that ME-Macs have an increased level of engulfed s129p$^+$ αS and upregulated autophagy and lysosomal clearance pathways. Furthermore, SAA results indicate that ME-Macs contain most of pathological misfolded αS compared with enteric neurons, suggesting the role of macrophages in misfolding and progression of pathological αS[19,24]. This raises the possibility that ME-Macs, although acting as a clearance mechanism, may also provide a microenvironment that promotes protein aggregation, consistent with observations of low-level physiological αS aggregates. Directed depletion of ME-Macs prevented the distribution of s129p$^+$ αS inclusions along myenteric neurons of the ENS and CNS. However, we note that our depletion strategy also caused a slight reduction in eosinophils and monocyte numbers. Further, ME-Macs express PD risk factors linked to endolysosomal pathways, including *Gba1*, *Lrrk2*, *Vps35* and *Ctsd*, the last involved in αS degradation[41]. These findings suggest that ME-Macs serve as early modulators of αS pathology. Of interest, microglia have been shown to phagocytose extracellular αS through the initiation of autophagy but then fail to clear the internalized αS in the brains of human αS-overexpressing mouse models[19,42]. These studies and our findings highlight tissue-resident macrophages along the gut–brain axis as key contributors to αS misfolding. Whereas our model uses direct administration of pathogenic αS fibrils, the endogenous triggers of αS aggregation in the human gut remain undefined[43]. Environmental and intrinsic factors may trigger αS aggregation in the gut. Pesticide exposure (for example, rotenone) induces enteric αS pathology in rodents[44]. Viral infections (for example, norovirus) upregulate αS expression, and ageing is associated with progressive accumulation and phosphorylation of αS in mice[44]. These mechanisms provide potential links between our models and human PD pathophysiology. Further research is needed to unravel the mechanisms governing αS uptake and degradation and to determine whether targeting specific pathways in microglia and ME-Macs can modify disease progression. Of note, pharmacological inhibition of LRRK2 reduces αS pathology and its propagation in neocortex, striatum and corpus callosum through enhanced lysosomal clearance of αS[45]. Further experiments are warranted to determine the role of ME-Macs in αS misfolding and the role of LRRK2 and GBA1 herein.

Our study in body-first PD models further suggests that early ME-Mac dysfunction promotes local T cell expansion, enabling their migration to the CNS. We further observed expansion of CD3$^+$ T cells in the ENS of body-first PD models. CD4$^+$ T cell infiltration has been observed in postmortem human PD samples[6]. Moreover, αS-overexpressing mouse models deficient in CD4$^+$ T cells are protected against midbrain neuronal loss, and recent work demonstrated αS-reactive circulating CD4$^+$ T cells in patients with early-stage PD, but with unknown origin[5,6,29]. Here we show that T cells can infiltrate and expand in ME of PD models, coinciding with αS propagation and spread to the CNS. Treatment with fingolimod mitigated neurodegeneration in PD-αS-injected mice, supporting the role for αS-induced T cell trafficking in disease progression; however, the broader immunomodulatory effects of fingolimod warrant further investigation to clarify specificity. CD3$^+$ T cells migrate from ME to the dorsal border of the striatum and lateral ventricle, possibly through the ependymal epithelial layer that intersects the ventricles and parenchyma. The ependymal layer was recently suggested as a potential entry site of infiltrating leukocytes and demonstrates an extensive amount of aggregated αS in patients with PD[46]. Alternatively, circumventricular organs lacking tight junctions and featuring fenestrations, such as the area postrema or subfornical organ, may serve as entry points for gut-derived immune cells[47]. However, the underlying mechanisms driving T cell trafficking and entry into the CNS, remain unclear. Peripheral T cells have been demonstrated to enter the CNS by means of recognition of a mitochondria-derived antigen, thereby driving dopaminergic neuronal loss in *Pink1*-deficient mice[35]. Systemic lipopolysaccharide induces the recruitment of T cells and monocytes to the brain in the context of αS pathology, suggesting that peripheral inflammation may act as a trigger for immune cell infiltration in PD[48]. Thus, T cell trafficking from the ENS to the CNS may be driven by αS-induced neuronal inflammation, coupled with human leukocyte antigen-associated αS peptide presentation by antigen-presenting cells in the CNS.

Finally, directed ME-Macs depletion reduces CD3$^+$ T cell expansion and αS pathology, raising key questions about the mechanisms by which ME-Macs and T cells communicate. First, the role of dendritic cells, as the quintessential antigen-presenting cells, remains unclear in this process. ME-Macs upregulate MHCII in the presence of αS pathology, consistent with the genetic association between the human leukocyte antigen region and PD, although this has not yet been specifically described for tissue-resident macrophages[49]. A critical future objective is to determine which lysosomal antigens are presented on MHCII by ME-Macs following αS engulfment. Alternatively, ME-Macs may transfer unprocessed antigens to dendritic cells for subsequent T cell priming. Of note, CD163$^+$ ME-Macs are enriched in perivascular-associated genes and are resemblant of border-associated macrophages in the CNS, recently implicated in the recruitment and activation of CD4$^+$ T cells in an αS-overexpressing mouse model[16,50]. Consistent with our findings and enhanced expression of MHCII on ME-Macs, depletion of BAM led to reduced expansion of CD4$^+$ T cells and prevention of disease progression[16]. The location and timing of ME T cell priming, particularly within secondary lymphoid organs such as Peyer's patches and mesenteric lymph nodes, remain to be elucidated. Notably, our findings suggest that TGFβ in ME-Macs has a key role in modulating T cell expansion in response to αS pathology, as depletion of TGFβ in ME-Macs ameliorated the αS-induced T cell increase. TGFβ is critical for driving T cell differentiation into either regulatory or Th17 phenotypes; yet cytokines such as IL-6 ultimately dictate the final fate of these T cells. Understanding these pathways will provide essential insights into the interplay between ME-Macs and T cells in synucleinopathy.

The gut–brain axis in PD has been extensively implicated in clinical settings, however, the cellular mediators involved in this process have been unclear. The unique properties of ME-Macs, such as their ability to engulf and modify αS aggregates, as well as their impact on T cell expansion and migration, highlight their significance in the earliest stages of αS pathology in PD. Targeting ME-Macs could offer potential therapeutic avenues for modulating αS pathology and its progression in PD or, alternatively, represent a valuable diagnostic biomarker for early immune changes in PD pathogenesis.

Online content

Any methods, additional references, Nature Portfolio reporting summaries, source data, extended data, supplementary information, acknowledgements, peer review information; details of author contributions and competing interests; and statements of data and code availability are available at https://doi.org/10.1038/s41586-025-09984-y.

1. Fasano, S. A., Visanji, N. P., Liu, L. W. C., Lang, A. E. & Pfeiffer, R. F. Gastrointestinal dysfunction in Parkinson's disease. *Lancet Neurol.* **14**, 625–639 (2015).
2. Horsager, J. et al. Brain-first versus body-first Parkinson's disease: a multimodal imaging case-control study. *Brain* **143**, 3077–3088 (2020).

3. Challis, C. et al. Gut-seeded α-synuclein fibrils promote gut dysfunction and brain pathology specifically in aged mice. *Nat. Neurosci.* **23**, 327–336 (2020).
4. Kim, S. et al. Transneuronal propagation of pathologic α-synuclein from the gut to the brain models Parkinson's disease. *Neuron* **103**, 627–641 (2019).
5. Lindestam Arlehamn, C. S. et al. α-Synuclein-specific T cell reactivity is associated with preclinical and early Parkinson's disease. *Nat. Commun.* **11**, 1875 (2020).
6. Sulzer, D. et al. T cells from patients with Parkinson's disease recognize alpha-synuclein peptides. *Nature* **546**, 656–661 (2017).
7. Tansey, M. G. et al. Inflammation and immune dysfunction in Parkinson disease. *Nat. Rev. Immunol.* **22**, 657–673 (2022).
8. De Schepper, S. et al. Self-maintaining gut macrophages are essential for intestinal homeostasis. *Cell* **175**, 400–415 (2018).
9. Muller, P. A. et al. Crosstalk between muscularis macrophages and enteric neurons regulates gastrointestinal motility. *Cell* **158**, 300–313 (2014).
10. Kalia, L. V. & Lang, A. E. Parkinson's disease. *Lancet* **386**, 896–912 (2015).
11. Braak, H. et al. Staging of brain pathology related to sporadic Parkinson's disease. *Neurobiol. Aging* **24**, 197–211 (2003).
12. Park, M. D., Silvin, A., Ginhoux, F. & Merad, M. Macrophages in health and disease. *Cell* **185**, 4259–4279 (2022).
13. Bain, C. C. et al. Constant replenishment from circulating monocytes maintains the macrophage pool in the intestine of adult mice. *Nat. Immunol.* **15**, 929–937 (2014).
14. Bogunovic, M. et al. Origin of the lamina propria dendritic cell network. *Immunity* **31**, 513–525 (2009).
15. Phillips, R. J., Billingsley, C. N. & Powley, T. L. Macrophages are unsuccessful in clearing aggregated alpha-synuclein from the gastrointestinal tract of healthy aged Fischer 344 rats. *Anat. Rec.* **296**, 654–669 (2013).
16. Schonhoff, A. M. et al. Border-associated macrophages mediate the neuroinflammatory response in an alpha-synuclein model of Parkinson disease. *Nat. Commun.* **14**, 3754 (2023).
17. Bido, S. et al. Microglia-specific overexpression of α-synuclein leads to severe dopaminergic neurodegeneration by phagocytic exhaustion and oxidative toxicity. *Nat. Commun.* **12**, 6237 (2021).
18. Nuber, S. et al. Abrogating native α-synuclein tetramers in mice causes a L-DOPA-responsive motor syndrome closely resembling Parkinson's disease. *Neuron* **100**, 75–90 (2018).
19. Bartels, T., De Schepper, S. & Hong, S. Microglia modulate neurodegeneration in Alzheimer's and Parkinson's diseases. *Science* **370**, 66–69 (2020).
20. Parker, W. D., Parks, J. K. & Swerdlow, R. H. Complex I deficiency in Parkinson's disease frontal cortex. *Brain Res.* **1189**, 215 (2008).
21. Palmieri, M. et al. Characterization of the CLEAR network reveals an integrated control of cellular clearance pathways. *Hum. Mol. Genet.* **20**, 3852–3866 (2011).
22. Concha-Marambio, L., Pritzkow, S., Shahnawaz, M., Farris, C. M. & Soto, C. Seed amplification assay for the detection of pathologic alpha-synuclein aggregates in cerebrospinal fluid. *Nat. Protoc.* **18**, 1179–1196 (2023).
23. Caputo, A. et al. Snca-GFP knock-in mice reflect patterns of endogenous expression and pathological seeding. *eNeuro* **7**, ENEURO.0007-20.2020 (2020).
24. Peng, C. et al. Cellular milieu imparts distinct pathological α-synuclein strains in α-synucleinopathies. *Nature* **557**, 558–563 (2018).
25. Damier, P., Hirsch, E. C., Agid, Y. & Graybiel, A. M. The substantia nigra of the human brain II. Patterns of loss of dopamine-containing neurons in Parkinson's disease. *Brain* **122**, 1437–1448 (1999).
26. Chen, Y. et al. Clinical characteristics and peripheral T cell subsets in Parkinson's disease patients with constipation. *Int. J. Clin. Exp. Pathol.* **8**, 2495 (2015).
27. Garretti, F. et al. Interaction of an α-synuclein epitope with HLA-DRB1*15:01 triggers enteric features in mice reminiscent of prodromal Parkinson's disease. *Neuron* **21**, 3397–3413 (2023).
28. Gate, D. et al. $CD4^+$ T cells contribute to neurodegeneration in Lewy body dementia. *Science* **374**, 868 (2021).
29. Williams, G. P. et al. CD4 T cells mediate brain inflammation and neurodegeneration in a mouse model of Parkinson's disease. *Brain* **144**, 2047–2059 (2021).
30. Rustenhoven, J. et al. Functional characterization of the dural sinuses as a neuroimmune interface. *Cell* **184**, 1000–1016 (2021).
31. Ugur, M., Kaminski, A. & Pabst, O. Lymph node γδ and αβ CD8+ T cells share migratory properties. *Sci. Rep.* **8**, 8986 (2018).
32. Henderson, J., Nagano, Y., Milighetti, M. & Tiffeau-Mayer, A. Limits on inferring T cell specificity from partial information. *Proc. Natl Acad. Sci. USA* **121**, e2408696121 (2024).
33. Chakarov, S. et al. Two distinct interstitial macrophage populations coexist across tissues in specific subtissular niches. *Science* **363**, eaau0964 (2019).
34. Browaeys, R., Saelens, W. & Saeys, Y. NicheNet: modeling intercellular communication by linking ligands to target genes. *Nat. Methods* **17**, 159–162 (2020).
35. Matheoud, D. et al. Intestinal infection triggers Parkinson's disease-like symptoms in *Pink1*$^{-/-}$ mice. *Nature* **571**, 565–569 (2019).
36. Zhai, S., Tanimura, A., Graves, S. M., Shen, W. & Surmeier, D. J. Striatal synapses, circuits, and Parkinson's disease. *Curr. Opin. Neurobiol.* **48**, 9–16 (2018).
37. Brinkmann, V. et al. Fingolimod (FTY720): discovery and development of an oral drug to treat multiple sclerosis. *Nat. Rev. Drug Discov.* **9**, 883–897 (2010).
38. Warner, T. T. et al. Genetic and environmental factors in the cause of Parkinson's disease. *Ann. Neurol.* **53**, S16–S25 (2003).
39. Peng, C., Trojanowski, J. Q. & Lee, V. M. Y. Protein transmission in neurodegenerative disease. *Nat. Rev. Neurol.* **16**, 199–212 (2020).
40. Alessi, D. R. & Sammler, E. LRRK2 kinase in Parkinson's disease. *Science* **360**, 36–37 (2018).
41. Videlock, E. J. et al. Distinct patterns of gene expression changes in the colon and striatum of young mice overexpressing alpha-synuclein support Parkinson's disease as a multi-system process. *J. Parkinsons Dis.* **13**, 1127–1147 (2023).
42. Choi, I. et al. Microglia clear neuron-released α-synuclein via selective autophagy and prevent neurodegeneration. *Nat. Commun.* **11**, 1386 (2020).
43. Mercado, G., Kaeufer, C., Richter, F. & Peelaerts, W. Infections in the etiology of Parkinson's disease and synucleinopathies: a renewed perspective, mechanistic insights, and therapeutic implications. *J. Parkinsons Dis.* **14**, 1301 (2024).
44. Kasen, A. et al. Upregulation of α-synuclein following immune activation: possible trigger of Parkinson's disease. *Neurobiol. Dis.* **166**, 105654 (2022).
45. Bae, E. J. et al. LRRK2 kinase regulates α-synuclein propagation via RAB35 phosphorylation. *Nat. Commun.* **9**, 3465 (2018).
46. Kovacs, G. G. Clinical neuropathology image 5-2014: α-synuclein pathology in the ependyma in Parkinson's disease. *Clin. Neuropathol.* **33**, 328 (2014).
47. Yoshida, T. M. et al. The subfornical organ is a nucleus for gut-derived T cells that regulate behaviour. *Nature* **643**, 499–508 (2025).
48. Peralta Ramos, J. M. et al. Peripheral inflammation regulates CNS immune surveillance through the recruitment of inflammatory monocytes upon systemic α-synuclein administration. *Front. Immunol.* **10**, 80 (2019).
49. Hamza, T. H. et al. Common genetic variation in the HLA region is associated with late-onset sporadic Parkinson's disease. *Nat. Genet.* **42**, 781–785 (2010).
50. Van Hove, H. et al. A single-cell atlas of mouse brain macrophages reveals unique transcriptional identities shaped by ontogeny and tissue environment. *Nat. Neurosci.* **22**, 1021–1035 (2019).

Methods

Mice

All experiments were performed in accordance with the UK Animals (Scientific Procedures) Act 1986 and following local ethical advice. Experimental procedures were approved by the UK Home Office and ethical approval was granted through consultation with veterinary staff at University College London (UCL). For all experiments, mice were obtained from the following sources and subsequently bred side by side in cages: C57BL/6J (WT) mice were obtained from Charles River UK, C57BL/6-Tg(Thy1-SNCA*E35K*E46K*E61K)3798Nuber/J (3KL) were obtained from The Jackson Laboratory. VHD (B6.tg(HD2)) mice were obtained from V. Cerovic (Institute of Molecular Medicine, RWTH Aachen). Sncatm1.1Kluk/J (*Snca*$^{WT/GFP}$) were obtained from K. Luk (Perelman School of Medicine, University of Philadelphia). *Cx3cr1*^{CreERT2}.*Tgfb1*^{LoxP} animals were obtained from M. Greter (University of Zurich). Different strains were bred in the same location to harmonize environmental factors. All animals were housed under temperature-controlled (temperature, 23.1 °C; humidity, 30–60%) and pathogen-free conditions with 12 h light–12 h dark cycle with an ad libitum supply of food and water. Both male and female age-matched mice were used in this study: WT, VHD, *Snca*$^{WT/GFP}$. Both male and female 3KL mice were used. Animals of 3–4 months were used for ME injection experiments.

Human tissue samples

All tissue samples were donated with the full, informed consent. Accompanying clinical and demographic data of all cases used in this study were stored electronically in compliance with the 1998 Data Protection Act. Ethical approval for the study was obtained from the NHS Research Ethics Committee and in accordance with the Human Tissue Authority's code of practice and standards under licence number 12198, with an approved material transfer agreement. Consent has been obtained for sharing of individual-level data. Use of Translational Pathology Core Laboratory-derived human tissues was approved by the University of California Los Angeles Institutional Review Board, which waived the informed consent requirement for specimens acquired from the Translational Pathology and Core Laboratory (TPCL) (IRB 11-002504). Specimens were deidentified and age was provided as a 5-year age range.

Tamoxifen treatment

Cx3cr1^{CreERT2}.*Tgfb1*^{LoxP} and littermate control mice were orally gavaged 3 times (every other day) with 5 mg of tamoxifen (Sigma-Aldrich T5648) dissolved in corn oil at around 6 weeks of age.

Tissue isolation for histology

Mice were deeply anaesthetized using pentobarbital and were transcardially perfused with 15 ml of ice-cold filtered PBS (Gibco) followed by 15 ml of ice-cold 4% paraformaldehyde (PFA) (ThermoFisher). To obtain tissue from the ME, the small intestine was isolated, stored in ice-cold PBS and cut open longitudinally. Ice-cold PBS was used to clean the tissue from luminal debris. The tissue was stretched on a Sylgard plate, and the ME was carefully peeled off using surgical tools. Isolated ME was further fixed in ice-cold 4% PFA for 20 min and preserved at −20 °C in cryoprotectant solution (10% sucrose, ethylene glycol) until stained. From the lamina propria (cross-sections), 2-cm long pieces of small intestine were isolated and luminal contents were gently flushed with ice-cold PBS using a syringe. The tissue was further fixed in 4% PFA at 4 °C overnight and excess PFA was washed with 3 × 10 min in ice-cold PBS. The tissue was dehydrated using 30% sucrose solution in PBS and frozen vertically in embedding moulds (Epredia) with optimal cutting temperature medium (Sakura) before cryo-sectioning. Sections of 20–25 µm were mounted on microscopy slides (Epredia) until staining. The brain was isolated from the skull and was further fixed, frozen and sectioned as described for cross-sections above. Sections were preserved at −20 °C in cryoprotectant solution until stained. To obtain whole mounts of dura mater, the skull cap containing the dura mater was removed from the mouse skull and stored fixed in ice-cold 4% PFA at 4 °C for 2 h. After fixation, the dura mater was carefully removed.

Tissue isolation for FACS and cell sorting

Mice were anaesthetized using pentobarbital and were transcardially perfused with 15 ml of ice-cold filtered PBS. Collected tissues were stored in ice-cold Roswell Park Memorial Institute medium 1640 (RPMI-1640) (Gibco) completed with 5% FBS (Gibco) and 20 mM HEPES (Gibco). To obtain single-cell suspensions from the ME, peeled ME was cut in 1–2-mm pieces and digested with 2 mg ml^{-1} Collagenase type IV and 0.8 mg ml^{-1} dispase in RPMI (Gibco) supplemented with 2% HEPES (Gibco), 2% FBS (Gibco) and 50 µg ml^{-1} DNase for 1 h at 37 °C with continuous agitation. The single-cell suspensions were then homogenized with a potter grinder and strained through 70-µm cell strainers (BD Falcon). From the lamina propria, the remaining tissue following isolation of the ME, containing the lamina propria and submucosa layers, was washed with ice-cold Hank's buffered saline solution (Gibco) supplemented with 1 mM dithiothreitol (Sigma-Aldrich), 1 mM EDTA (Invitrogen) and 20 mM HEPES for 8 min. Single-cell suspensions of lamina propria were prepared by digestion with 0.85 mg ml^{-1} Collagenase Type V (Sigma-Aldrich) in MEMα (Lonza) supplemented with 2% HEPES, β-mercaptoethanol (Gibco) and DNase for 30 min at 37 °C with continuous agitation. For the brain and dura, brains were quickly isolated from the skull, and brainstem was dissected from the rest of the brain tissue on ice using chilled instruments. The dorsal part of the skull was carefully removed, and meningeal dura mater was peeled off of the skull cap. The tissues were finely chopped using chilled razorblades and transferred to tubes containing ice-cold RPMI-1640 supplemented with 10% FBS and 20 mM HEPES medium. Single-cell suspensions from brainstem were prepared using the Dissociation kit (Miltenyi Biotech) according to the manufacturer's instructions. Tissue chunks were pelleted by centrifugation at 300*g* for 2 min at 4 °C followed by medium removal and resuspension in a mix of buffer Z with enzymes A, P and Y. For digestion of meningeal dura mater, chopped tissue was resuspended in 0.5 mg ml^{-1} Collagenase P, 0.8 mg ml^{-1} Dispase II and 250 U ml^{-1} DNase1 and digested for 30 min. Single-cell suspensions from all tissues were then blocked with rat anti-mouse CD16/CD32 antibodies (BD Biosciences) used at the recommended dilution for 12 min before incubation with primary antibodies diluted at recommended dilutions (Supplementary Table 3) in FACS buffer (PBS, 2% FBS, 0.78 mM EDTA) containing Fc block for 20 min at 4 °C. Dead cells were excluded using Live/Dead near-infrared dye staining (Invitrogen) diluted in PBS or 4,6-diamidino-2-phenylindole (DAPI). Precision Count Beads (BioLegend) were used for absolute cell counting and analysed using the following formula: absolute cell count (cells per µm) = cell count/beads count × bead concentration. Flow cytometry data were analysed using FACSDiva software (v.4.0) and FlowJo software (Treestar).

Cell sorting was performed on a BD Aria III (BD Biosciences). For scRNA-seq (Fig. 4) and proteomics (Fig. 1), live CX3CR1^{hi}CD11b^{+}CD11c^{-} ME-Macs and CD3^{+} cells (Extended Data Fig. 6a) were sorted in DMEM supplemented with 30% FBS and resuspended in PBS with 0.04% BSA.

Immunofluorescence

For free-floating sections, fixed ME or brain sections were permeabilized with 0.5% (ME) or 0.3% (brain) Triton X-100 at room temperature for 1 h followed by blocking with blocking buffer (5% donkey or goat serum (Abcam) and 0.5% or 0.3% Triton X-100 (ThermoFisher Scientific)) at room temperature for 1 h. Primary antibodies diluted at their recommended concentrations (Supplementary Table 3) in blocking buffer were added and the tissue was incubated at 4 °C overnight. Following 4 15-min PBS washes, the tissue was incubated with secondary antibodies diluted in blocking buffer for 2 h at room temperature and was washed again with PBS. Secondary antibody aliquots were centrifuged at 15,000*g* for 15 min before dilution in blocking buffer. Tissue

was incubated for 5 min with DAPI (Roche) before being mounted on Prolong Gold Antifade Mounting Medium (ThermoFisher Scientific). For on-slide staining, for the gut cross-sections, slides were washed in PBS to remove excess optimal cutting temperature medium before permeabilizing with 0.3% Triton and blocking with 5% goat or donkey serum for 15 min. For dura mater whole-mount images, sections were washed 2 times with PBS and blocked for 1.5 h at room temperature with 10% normal donkey serum (Sigma-Aldrich) in PBS containing 0.3% Triton (Sigma-Aldrich) (PBS-T). Subsequently, the sections were stained with primary antibodies in 3% normal donkey serum/PBS-T (overnight, 4 °C). The following day, the samples were washed three times with PBS-T and once with PBS. The tissues were then stained with DAPI (Sigma-Aldrich)/PBS solution for 30 min at room temperature and washed twice with PBS. Finally, the sections were mounted using Mowiol 4-88 (Polysciences Inc.) mounting solution (prepared according to the manufacturer's instructions) and stored at 4 °C. Dura mater whole mounts were imaged using a Phenoimager (Akoya Biosciences), or Nikon SoRa Spinning Disk Confocal using a ×10/×20 objective for large overview images and ×40/×60 objective for zoom-ins, all other tissues were analysed using a LSM800 (Zeiss), a LSM980 or Leica Stellaris STED microscope using a ×100 1.4 numerical aperture (NA) oil immersion Plan-Apochromat objective. All images were processed and analysed with Fiji (National Institutes of Health, NIH) and QuPath[51]. For T cell quantification (Figs. 3–5), we analysed 1–2 regions of interest (ROIs) (159.72 µm × 159.72 µm) per 4–5 adjacent ganglia in the duodenum, with data represented per ROI. Glial fibrillary acidic protein-positive myenteric glial cells were 3D-reconstructed using Imaris software (Bitplane), and their volume was calculated following background subtraction. For each mouse, four ROIs were analysed per ganglion. HuC/D$^+$ neurons were quantified in two adjacent ganglia within the duodenum, with a ganglion defined as a cohesive aggregate of HuC/D-positive cells. Extraganglionic cells were excluded from the analysis.

Single molecule fluorescence in situ hybridization (smFISH) (RNAscope) and smFISH combined with IHC

To detect single RNA molecules, the RNA probe for *Tgfb1* (407751) as well as the RNAscope Multiplex Fluorescent Detection Reagents v2 (323110) kit were purchased from ACD BioTechne. ME tissue was cryosectioned at 20 µm and was collected on Superfrost Plus Gold Slides (ThermoFisher K5800AMNZ72) and dried at room temperature overnight. The assay was performed according to the manufacturer's instructions, and the standard IHC protocol as described above was used.

Brain IHC

Free-floating 15-µm or 25-µm (for brainstem and dorsal motor nucleus of the vagus) or 30-µm (SNpc) serial coronal sections were cut with a Leica CM1860 cryostat. The tissue was then treated with 0.3% H_2O_2 for 30 min. For staining with mouse anti-s129p antibodies, the samples were then incubated in M.O.M. blocking solution from mouse-on-mouse Elite Peroxidase Kit (Vector laboratories, PK-2200) prepared according to the manufacturer's instruction for 1.5 h. The tissue was then blocked for another 5 min in M.O.M. diluent from the kit. Then, the sections were incubated with primary antibodies against s129p αS (1:10 000; BioLegend, clone P-syn/81A, 825701) for 12 h at 4 °C. The following day, the sections were treated with M.O.M. Biotinylated Anti-Mouse IgG Reagent from M.O.M. Elite Peroxidase Kit (PK-2200) prepared according to the manufacturer's instructions for 1 h at room temperature, and subsequently transferred into ABC solution (Vectastain Elite ABC Kit, Vector Laboratories) for 10 min at room temperature, and visualized with 3,3′-diaminobenzidine (DAB) (DAB Substrate Kit, Vector Laboratories). Sections were then transferred onto the glass slides, air dried, sequentially dehydrated in PBS, 70%, 100% ethanol and 100% xylene, and mounted. The images were taken on an Axioscope 5 microscope (Zeiss). For staining with rabbit anti-s129p antibodies, the free-floating sections were treated with 0.3% triton for 30 min, 0.3% H_2O_2 for 30 min and blocked in 20% normal goat serum, 1% BSA, 0.3% triton for 1 h at room temperature. The samples were then incubated with primary antibodies against s129p αS (1:20 000; Abcam, EP1536Y) for 12 h at 4 °C. After washing with PBS, the sections were incubated with the biotinylated secondary antibodies (1:200, Vector, Goat Anti-Rabbit IgG Antibody (H+L), Biotinylated, BA-1000-1.5) for 1 h at room temperature, subsequently transferred into ABC solution (Vectastain Elite ABC Kit, Vector Laboratories, PK-6100) for 45 min at room temperature and visualized with DAB (DAB Substrate Kit, Vector Laboratories).

s129p αS analysis

Fiji (NIH) was used to measure the total area of s129p αS signal in the total myenteric plexus and brainstem.

Myenteric plexus. Individual channels were first *Z*-projected and background-subtracted (10-pixel rolling ball radius). Next, threshold channels were empirically determined and then consistently applied to each channel for all subjects. For quantifying s129p, the Analyze Particles tool in ImageJ was used to quantify the total area of s129p (per myenteric ganglia or calculated per mm^2). For the brainstem (for immunofluorescence), *Z*-stacks were taken of the entire tissue thickness within the dorsal motor nucleus of the vagus at 1-µm *Z*-step increments. Images were analysed in Fiji (NIH), in which individual channels were first *Z*-projected and thresholded empirically and a median filter of 0.5 pixels was applied to determine only punctate staining of total and s129p αS. This was consistently applied to each channel for all subjects. ROIs were drawn around choline acetyltransferase-positive cells with the freehand selections tool. The Analyze Particles tool in Fiji was used to quantify the total number of puncta and the percentage of punctate staining within each choline acetyltransferase-positive cell by applying ROIs to the corresponding total and s129p αS channels. For the brainstem (for DAB), first, colour deconvolution with H DAB vectors was used. Then, the background was subtracted with a rolling ball radius of 50 pixels from the images, followed by adjusting the threshold to measure the fibrillar inclusions of s129p αS. Total signal area was measured for each image, and the data were normalized to the average of the control group in each staining batch. Alternatively, the optical density of the DAB signal was measured in Fiji by first calibrating the software according to the ImageJ User guide. The optical density of individual cell bodies was then measured and the background optical density was subtracted. Mean values for each mouse were then calculated.

SNpc. *Z*-stacks were taken of the entire tissue thickness within the SNpc at 1-µm *Z*-step increments. Images were analysed in Fiji (NIH), where channels were split, the tyrosine hydroxylase (TH) channel was *Z*-projected and ROIs were drawn around TH$^+$ cells as well as at least one ROI to measure background fluorescence. These ROIs were applied to the total and s129p αS channels and area, mean fluorescence and integrated density were measured for each cell at each plane of the *Z*-stack. Corrected total cell fluorescence (CTCF) for each TH$^+$ cell was determined with the following equation: CTCF = integrated density − (area of selected cell × mean fluorescence of background readings). For SNpc s129p αS analysis, data were normalized to total αS and all data were then normalized to the mean of the NHC-αS group value.

TH and Nissl IHC

For TH IHC, brains were sagittally hemisected at the midline following removal of the hindbrain. The left hemisects were embedded in 10% sucrose, 0.5% glutaraldehyde in chicken egg yolk. The sample was allowed to polymerize for 5 min before being stored at −80 °C until sectioning. Embedded brains were sectioned into 30-µm slices using a Leica CM1860 cryostat and stored in cryoprotection solution at −20 °C until used for staining. All staining was performed in free-floating baskets (made in-house). Free-floating sections were washed once in PBS

pH 7.5 for 5 min at room temperature on a horizontal rocker. Sections were then blocked in 5% BSA + 0.3% Triton X-100 in PBS for 1 h at room temperature. Following 3 × 5 min wash in PBS, sections were incubated in anti-TH antibody (Immunostar 22941) diluted 1:1,000 in 2% BSA + 0.1% Triton X-100 in PBS for roughly 16 h at 4 °C. Following 3 × 5-min washes in PBS, sections were incubated in biotinylated anti-mouse secondary antibody for 2 h at room temperature. Avidin-biotin complex elite kit (ABC, Vector labs PK-6100) (1:50 in PBS) was prepared 30 min before use according to the manufacturer's instructions. Sections were then washed 3× for 5 min in PBS and incubated for 1 h at room temperature in ABC. Following a final 3 × 5-min wash in PBS, sections were incubated for 10 min in DAB solution (1 tablet Sigma D4418-50 set, 15 ml of PBS + 4.5 µl of H_2O_2). Sections were then washed once in PBS (5 min) and once in dH_2O before being mounted onto slides and dried for roughly 30 min at 37 °C, and then covered with a glass coverslip with a polyvinyl alcohol-based mounting media (made in-house). All counting was performed blinded for treatment type and images were taken using a ×20 objective on a Leica Mica microscope acquiring *z*-stacks with a 0.7 µm *z*-step size. Stacked image tiles were loaded into StereoInvestigator desktop (MBF Bioscience). Stereological quantification was performed using the optical fractionator method from StereoInvestigator, analysing every sixth 30-µm coronal section serially for the SNpc and VTA ROIs. Using a counting frame of 50 × 50 µm snapped to 1-µm increments and a systematic random sampling grid size of 100 × 100 µm, TH^+ cells were quantified unbiasedly[52,53].

For Nissl staining, mounted sections containing SNpc and VTA used in the TH^+ cell body quantifications were Nissl stained on top using a cresyl violet acetate-based solution to stain Nissl bodies (nucleoli and rough ER) purple. Slides were washed for 5 min in dH_2O and then submerged in Nissl staining solution (4.5 g cresyl violet acetate, 45 ml of 100% ethanol, 450 ml of distilled water) for 8 min before destaining for 10 s in 2% acetic acid in ethanol, 30 s in 100% ethanol and 1 min in 100% ethanol. Sections were cleared in xylene for 10–15 min, before mounting with DPX mounting media (Cellpath SEA-1304-00A) and glass coverslips. TH^+ neurons and $Nissl^+$ neurons only (not glial cells) were quantified by unbiased stereology using the same parameters as the TH^+ cell body quantifications[53,54]. The Nissl stain is most intense in nucleoli and in the rough endoplasmic reticulum of neurons and less in glia cells, enabling differentiation on the basis of staining patterns.

Nanostring DSP

Here, 5-µm-thick formalin-fixed paraffin-embedded sections of the myenteric plexus were deparaffinized and incubated with antibodies against bIII-tubulin to select myenteric ganglia as segmented ROI, according to the manufacturer's instructions and ref. 55. Cell nuclei were stained with DAPI. Each ROI was manually drawn around myenteric ganglia in the myenteric plexus (geometric segments), encompassing both neurons and glial cells, resulting in a total of 2–3 analysed ROIs per slide. Each slide was incubated with an antibody panel conjugated to a unique UV-photocleavable oligonucleotide tag. Selected ROIs were individually illuminated with UV light using NanoString's GeoMx Digital Spatial Profiler System (NanoString Technologies). Cleaved oligonucleotides were collected in 96-well plates and optical barcodes were analysed using the NanoString nCounter system. Obtained digital counts were normalized for signal-to-noise ratio using Rat IgG2b and Rabbit IgG. Internal housekeeping proteins included Histone H3, S6 and GAPDH.

TCR sequencing and analysis

RNA extracted was extracted from tissue samples and the TCR α and β genes were sequenced using an established quantitative sequencing pipeline, which uses unique molecular barcodes to correct for PCR bias, and sequencing errors[56,57]. The fastq files were processed and annotated using the in-house open-source computational pipeline Decombinator V5 (ref. 58). Plots were prepared using Python v.3.12.4, Plotly and Scipy. The NHC-αS- and PD-αS-injected groups were compared using a Bonferroni-adjusted unpaired *t*-test with Welch's correction. The Jaccard index is defined as

$$J = \frac{|A \cap B|}{|A \cup B|} \quad (1)$$

where A and B are each a set of clonotypes in a tissue. To compute the expanded index, let $c(\sigma)$ be the count of clonotype σ transcripts in the sample it is found in, and E_A be the expanded subset of A such that

$$E_A = \{c | c(\sigma) > 1 \ \forall \ \sigma \in A\} \quad (2)$$

Then the expanded index is computed by

$$\varepsilon = \frac{|E_A \cap B|}{|E_A|} \quad (3)$$

Mass spectrometry on sorted ME-Macs

Protein lysates from sorted duodenal ME-Macs were digested using the single-pot, solid-phase-enhanced sample-preparation method[59]. Samples were processed in accordance with the published methodology. Briefly, samples were reduced and alkylated using tris(2-carboxyethyl) phosphine and iodoacetamide, respectively. Alkylated proteins were then bound to the Sera-Mag SpeedBeads (ThermoFisher Scientific) by raising the organic solvent content of the buffer to above 70%. Proteins could then be washed using ethanol and acetonitrile before digestion within the same sample tube to reduce protein loss. Proteins were digested through the addition of 100 ng of Trypsin/Lys-C mix (Pierce) in 50 mM ammonium bicarbonate and leaving it at 37 °C at 300*g* overnight. Digested peptides were cleaned by binding them to the beads by means of increasing the organic solvent content of the buffer to above 95%. Samples were washed using 100% acetonitrile before being eluted from the beads using 2% DMSO. Peptide samples were then acidified to a final concentration of 0.1% Formic acid before injection onto the mass spectrometer. Acidified peptide samples were analysed on a Bruker TIMS-TOF Pro 2 using an EvoSep One. Samples were prepared onto an EvoTip in accordance with the manufacturer's instructions. Samples were loaded onto the mass spectrometer using the '20 samples per day' HPLC method provided by EvoSep using 100% water as a buffer A and 100% Acetonitrile as buffer B. The samples were acquired in data-independent acquisition mode with trapped ion mobility spectrometry on. Resultant data files were searched using DIA-NN v.1.8 (ref. 60). Search was performed against the UniProt SwissProt Mouse database in direct search mode. The double-pass neural network classifier was used and protein inference was using the protein IDs from the FASTA file. Precursor ion generation for the library used the default settings with a precursor false discovery rate at 1%. Mass accuracy and MS1 accuracy were set at 10 ppm each and the match between runs setting was enabled. Differential analysis data were analysed and visualized using CURTAIN v.2.0 (ref. 61).

Whole gastrointestinal transit function

An amount of 6% carmine red dye containing 1% methylcellulose was administered by oral gavage in 3-month-old 3KL mice or at 1 month and 3 months post-ME injection to determine the total gastrointestinal transit time. This parameter represents the time required for the mice to expel faeces containing the carmine red dye, starting from the moment of oral gavage.

Directed depletion of ME-Macs

Depletion of ME-Macs was carried out using a published protocol adapted to our purpose[9]. Mice were injected with 15 µg g^{-1} αCSF1R (clone AFS98, Bio XCell) versus IgG2a control (clone 2A3, Bio XCell)

into the ME, 24 h before injection with NHC-αS versus PD-αS. Mice were orally gavaged with 15 µg αCCR2 (MC21, kindly provided by M. Mack, Universität Regensburg) daily for 7 days after AFS98 treatment to restrain ME-Mac replenishment.

Fingolimod treatment

T cell egression was targeted by oral administration of fingolimod (FTY720, Cambridge Biosciences) at a dose of 0.5 mg kg^{-1} through gavage on days 1, 3, 5 and 7 following PD-αS treatment. Fingolimod was dissolved in ethanol (2 mg ml^{-1}) and saline. Saline containing 2 mg ml^{-1} ethanol was used as vehicle control.

Quantification of s129p αS engulfment

Engulfment analysis was performed as previously described but adapted to ME[62]. Mouse ME was immunostained with MHCII, LAMP1 and s129p αS, and human ME was immunostained with CD209 (ref. 63), LAMP1 and 2F12. Two regions and 3–6 ROIs were acquired for each mouse and human sample, respectively, on a ×63 1.4 NA objective Zeiss 800 microscope. For mouse, 60–80 *z*-stack planes were taken with 0.27-µm spacing and raw images were processed in Imaris (Bitplane) for analysis, after background subtractions. A mask was applied in $MHCII^+$ $LAMP1^+$ reconstructed lysosomes for s129p αS, and the percentage engulfment of s129p αS within lysosomes was calculated using the following formula: volume of engulfed material (s129p or 2F12 within LAMP1)/total ME-Mac volume × 100.

Sequential extraction of insoluble fraction from human brain

Sequential extraction from human brain was performed according to ref. 24. Briefly, 0.5 mg of brain tissue was homogenized in high salt (HI) buffer (50 mM Tris-HCl, 750 mM NaCl, 5 mM EDTA, 10 mM NaF, pH 7.40) containing protease inhibitors. After ultracentrifugation at 100,000*g* for 30 min at 4 °C, supernatant was removed and fresh HI buffer added. The same steps were subsequently repeated with HI buffer containing 1% Triton, HI buffer with 1% Triton and 30% sucrose, HI buffer with 1% sarkosyl and finally in PBS to resuspend the sarkosyl-insoluble fraction of the brain homogenate enriched in aggregated αS. In the absence of pathology, the sample is expected to contain minimal random contaminants, with samples showing comparable total αS levels between disease and NHC groups[64]. Postmortem brain samples used in this study are summarized in Supplementary Table 1b.

αS SAA

Flash-frozen PD brain tissue (500 µg, frontal cortex, Braak VI, absent copathology) was homogenized and subjected to serial extraction as described earlier. For the SAA reaction to amplify and monitor αS aggregates, 10 µl of brain-derived seed was incubated with recombinant monomeric αS at 42 °C in a BMG FLUOstar Omega plate reader to amplify amyloid αS by incorporating monomeric αS into the growing aggregate[22]. Before each SAA experiment, lyophilized monomeric protein was dissolved in 40 mM phosphate buffer (pH 8), filtered using a 0.22-mm filter and the concentration of recombinant protein was measured by use of absorbance at 280 nm using a Nanodrop One spectrophotometer. Brain-derived insoluble protein was tip-sonicated for 30 s (1 s off, 1 s on) at 30% of amplitude and added to a 96-well plate with 230 mM NaCl, 0.4 mg ml^{-1} αS and a 3-mm glass bead (Millipore Sigma, no. 1040150500). Repeated shaking (1 min incubation, 1 min double-orbital shaking at 400 rpm) disrupts the aggregates to produce an expanded population of converting units. The amyloid dye thioflavin T was used in adjacent wells to monitor the increase in fibrillar content through fluorescence readings at 480 nm every 30 min until the signal plateaued towards the end of the amplification interval of 4 days. The lag time of each sample was defined as the time at which the average, background corrected thioflavin T fluorescence of the sample reached 5% of its own maximum fluorescence. For SAA on isolated ME-Macs and neurons, single-cell suspensions were isolated from the ME using the magnetic-activated cell sorting method (Miltenyi Biotec, 130-097-142). ME tissues were first homogenized as described earlier and centrifuged at 400*g* for 7 min. The resulting cell suspension was incubated with a CD11b antibody (Miltenyi Biotec) for 30 min at 4 °C to label $CD11b^+$ cells. The suspension was then passed through a magnetic-activated cell sorting magnetic column, and the flow-through containing $CD11b^-$ cells was collected for subsequent neuronal isolation. For the isolation of enteric neurons, $CD11b^-$ cells were processed using the Adult Neuron Isolation Kit (Miltenyi Biotec, catalogue no. 130-126-602). Briefly, cells were incubated with the Adult Non-Neuronal Cell Biotin-Antibody for 30 min, followed by centrifugation at 400*g* for 7 min. The pellet was incubated with anti-biotin microbeads for 10 min and subsequently applied to a magnetic-activated cell sorting magnetic column. The flow-through from this step represented the enriched enteric neuronal fraction. Isolated ME-Macs and enteric neurons were then lysed to obtain protein extracts. Tip sonication was performed for 30 s (1 s off, 1 s on) at 30% amplitude to ensure efficient lysis. Lysed cells were subjected to SAA as described above.

Recombinant αS expression and purification

Briefly, plasmid pET21a-SNCA was expressed in BL21(DE3) *Escherichia coli*. After cell lysis, αS was purified by use of ion exchange chromatography (5 ml HiTrap Q HP columns, GE Life Sciences, 17516301) and size exclusion chromatography (13 ml of HiPrep 26/60 Sephacryl S-200 HR, GE Life Sciences) using the ÄKTAprime plus fast protein liquid chromatography system and subsequently lyophilized in protein low binding tubes (Eppendorf)[65].

αS ELISA

Samples were processed and analysed as described before using 2F12 (MABN1817, Merck) as a capture, SOY1 (Merck, MABN1818) as a sulfo-tagged detection antibody on an MSD enzyme-linked immunosorbent assay (ELISA) platform[65]. For sulfotag labelling of detection antibodies, 200 µl of SOY1 antibody (1.37 mg ml^{-1} in PBS) was incubated at room temperature for 2 h with 16 µl of 3 nmol $µl^{-1}$ MSD NHS-Sulfotag reagent (150 nmol freshly suspended in 50 µl of PBS). Next, 250 µl of PBS was added to antibody solutions, concentrated using Amicon ultra filter tubes (10,000 molecular weight cut off), and brought up to 500 µl of PBS again. This was repeated five times to dilute out the tag reagent. Protein concentration was subsequently measured using BCA assay. For plate preparation, MSD Standard plates were coated with 30 µl of 200 ng filtered 2F12 (1 mg ml^{-1}) from recently filtered batches diluted in PBS and stored overnight at 4 °C. Plates were then tapped out, blocked with 150 µl per well in 5% MSD blocker A in 0.01% PBS-T, sealed and placed on an orbital shaker for 1 h at room temperature. Plates were subsequently washed 5 times with 150 µl of PBS-T per well, samples were added in 2% SDS in PBS-T with 1% MSD blocker A, as well as recombinant αS at different concentration gradients in PBS-T with 1% MSD blocker A (0.5% NP-40) (Meso Scale Diagnostics LLC) and incubated for 2 h at room temperature with orbital shaking. Plates were washed 5 times with 150 µl of 0.1% PBS-T per well before the addition of detection antibody solution: that is, 30 µl per well of 200 ng sulfo-tagged SOY1 antibody in PBS-T with 1% MSD blocker A. Plates were incubated for 1 h at room temperature with orbital shaking and protected from light. After 5 washes with PBS-T, 150 µl of 2× MSD reader buffer diluted in MilliQ water was added and the plate was read using a Meso Sector S 600.

Proteinase K digest

Sarkosyl-insoluble and SAA-amplified samples were treated with 1 µg ml^{-1} of proteinase K (Roche, 3115836001) at 37 °C for 1 h with gentle shaking. The digestion was stopped by adding NuPAGE LDS sample buffer (Invitrogen, NP0007) and boiling the sample at 95 °C for 7 min. Samples were then loaded onto a Novex 16% Tricine gels (Invitrogen) for protein separation. After electrophoresis, gels were incubated in

20% ethanol for 5 min at room temperature and blotted onto iBlot 2 Nitrocellulose Regular Stacks (Invitrogen) using the iBlot 2 Dry Blotting system (Invitrogen). The membrane was rinsed in ultrapure water and incubated in 4% PFA/PBS for 30 min at room temperature. The membranes were blocked in Odyssey blocking buffer (PBS)/PBS buffer 1:1 (LI-COR) or casein buffer 0.5% (BioRad) for 1 h at room temperature. After blocking, membranes were incubated overnight at 4 °C with anti-αS clone 42 (BD Biosciences). After three washes in PBS-T 0.1%, the membrane was incubated for 1 h at room temperature with the secondary antibody (goat anti-mouse IgG F(Ab)2 conjugated with horseradish peroxidase (HRP), Abcam) in blocking solution. Membranes were washed in PBS-T 0.1% and then the signal was detected using the Invitrogen iBright imaging system and the Luminata Crescendo Western HRP substrate (Millipore).

Endotoxin analysis of insoluble fractions

Lipopolysaccharide levels were measured with Pierce Chromogenic Endotoxin Quantification Kit (ThermoFisher, no. A39552). All experiments were conducted within a Laminar Flow cabinet using pyrogen (endotoxin) free pipette tips. The pH of each sample was measured using pH Strips and adjusted to within 6–8 using endotoxin-free sodium hydroxide (Merck) or hydrogen chloride (Merck). Before starting the assay all samples and kit components were left to warm to room temperature. The *E. coli* endotoxin standard vial was reconstituted with room temperature endotoxin-free water by adding 1:10 ml of the EU amount indicated on the vial to make a 10 EU ml^{-1} solution, then vortexed at 1,200 rpm for 15 min. Standards were prepared according to table 2 in the manufacturer's instructions. Samples were diluted to between 1:2 and 1:30 (10–50 µl of sample) with room temperature endotoxin-free water. Lyophilized Amoebocyte was reconstituted immediately before loading the plate with 1.7 ml of endotoxin-free water. Next, 50 µl of each standard, and samples were loaded in triplicate onto prewarmed plate (plate kept at 37 °C on a Thermoblock for the duration of the assay). Following sample and standard loading, 50 µl of reconstituted amoebocyte was added to each well. The plate was covered and left to incubate based on the manufacturer's instructions. Before the amoebocyte incubation window closing, chemogenic substrate was reconstituted with 3.4 ml of endotoxin-free water and incubated at 37 °C for 5–10 min. When amoebocyte incubation was finished, 100 µl of warm chemogenic substrate was added to each well and plate was left to incubate at 37 °C for 6 min. Finally, 25% acetic acid was added to each well (diluted in endotoxin-free water). The plate was read at an optical density of 405 nm before analysis.

Transmission electron microscopy

Transmission electron microscopy specimens were prepared on carbon-coated formvar grids (Electron Microscopy Sciences). Samples were adsorbed on the grids for 5 min and then negatively stained with 1% (w/v) aqueous uranyl acetate. Images were taken on a JEOL 1400 transmission electron microscope (JEOL USA Inc.) at an accelerating voltage of 100 kV.

Microinjections of human αS extracts into ME

Mice were anaesthetized with isoflurane (2–4%) and kept at constant body temperature with a conventional heat pad. Abdominal hair was removed, and an incision was made along the midline. A 10-µl 36 G Hamilton syringe (World Precision Instruments) was used to inject a total of 7 µl of human brain insoluble fraction (containing roughly 87 pg fibrillar αS by ELISA, Extended Data Fig. 3a) into the wall of the duodenum at 4 sites. The injection sites were located 0.5–1 cm away from pyloric stomach and at least 0.3 cm from each other. Injection sites were marked with 0.2% Fast Green FCF (Sigma-Aldrich). Following the injections, animals were sutured and single housed for 5 days to allow recovery. Animals received carprofen (33.33 mg ml^{-1}) in their drinking water for 4 days postsurgery. Mice were euthanized at 1 month or 3 months postinjection.

scRNA-seq library preparation, expression and NicheNet analysis

For scRNA-seq, four biologically independent samples (duodenal ME) were used per genotype, and one sample represents pooled ME from four mice. Single-cell libraries were prepared using 10X Genomics Chromium Next GEM Single Cell 5′ kit v.3.1, according to the manufacturer's instructions. Libraries were sequenced using an S2 flowcell on an Illumina NovaSeq S6000 instrument, with sequencing parameters recommended by 10X Genomics, aiming for 40,000 reads per cell. Raw Fastq read files were processed using cellranger count (v.6.0) for each dataset to generate count matrices that were used for subsequent analysis (filtered_feature_bc_matrix). Integrated analysis of multimodal single-cell data in R (v.4.0) were used to first examine each dataset individually using Seurat (v.4.3) and SeuratObject (v.4.1.3)[66]. Cells expressing fewer than 200 or more than 2,500 features were excluded from further analysis, as well as cells expressing more than 30% mitochondrially encoded features ('MT' chromosome in GRCm39). Each dataset was normalized individually using SCTtransform (v.0.4.1) and datasets were integrated together (IntegrateData) using 3,000 genes. Principle component analysis was carried using the 'RunPCA()' command on 100 principal components and the appropriate number of principal components evaluated using the and ElbowPlot function. Clusters of transcriptionally related cells were identified using the Louvain method and the 'FindClusters' command at 0.2 resolution and were visualized using uniform manifold approximation and projection for dimension reduction. Cell clusters corresponding to macrophages were identified through the expression of marker genes *Csf1r*, *Aif1* (*Iba1*), *Fcgr3* (CD16) and *H2-Eb1* (MHCII). T cells were identified through expression of *Cd3e* (CD3), *Cd8a* (CD8) and *Cd4*. Cell clusters that did not express any of these markers above were not considered for further analyses. Differentially expressed genes were computed for each cluster using the 'FindMarkers' command. ClusterProfiler (v.4.12.6) was used for Gene Ontology analysis considering differentially expressed genes with $\log_2$ fold change greater than 0.75 and Bonferroni-adjusted *P* value less than 0.05. Ligand–receptor interaction networks were inferred using nichenetr (v.2.2.0) considering differentially expressed genes in the receiver population (T cells) and the top ten ligands based on the area under the precision–recall curve expressed by 3KL macrophages.

Mouse multiplex cytokine array

Mice were anaesthetized and perfused with ice-cold PBS. The gut was dissected, and 75 mg of duodenal tissue was collected in 300 µl (4 times wet weight) ice-cold PBS with cocktail protease inhibitors (ThermoFisher Scientific, 11814111). The tissue was homogenized at 50 Hz for 5 min using a TissueLyser LT (Qiagen) and centrifuged at 10,000*g* for 10 min at 4 °C. The supernatant was collected and mixed well in an equal volume of RIPA lysis buffer (Thermo Scientific, 10017003), and left for 20 min on ice. The samples were then centrifuged at 10,000*g* for 10 min at 4 °C and the supernatant was collected and sonicated (70% amplitude, 30 s on and 30 s off for 10 min) (Q800R3 Sonicator, QSONICA). A standard BCA protein assay was performed on the supernatant fraction to obtain the amount of protein (ThermoFisher Scientific, 10678484). Cytokine levels were assessed using the proteome profiler array (Mouse Cytokine Array Panel A, BioTechne, ARY006), which detects the levels of 40 mouse cytokines. The analysis was performed using the manufacturer's instructions and 200 ng ml^{-1} of the samples were used. The dot blots were visualized by chemiluminescence detection using an Amersham Imager 680 (Bioke) system.

ME photoconversion

For photoconversion of ME T cells, VHD mice were first injected with NHC-αS versus PD-αS into ME. Five days later, mice were re-anaesthetized and small intestine was exposed to the site of injection,

marked with 0.2% Fast Green FCF (Sigma-Aldrich). The rest of the body was carefully covered with aluminium foil to avoid undesired exposure. Next, the intestine was illuminated with UV light (405 nm) 1 cm distally from injection site for total of 2 min (2 intervals of 60 s each) using a BlueWave QX4 high-intensity spot-curing system (DyMax) equipped with a 3 mm diameter focusing lens. During the illuminations, the intestine was kept wet with PBS. Abdominal incisions were carefully closed with separate sutures on both peritoneal layer and skin. Animals received carprofen (33.33 mg ml^{-1}) in their drinking water for 4 days postsurgery. Animals were euthanized at 1 month postsurgery.

Human gut tissue IHC

Postmortem formalin-fixed paraffin-embedded jejunal sections (ten from patients with PD, ten from NHC participants) were obtained from the Banner Sun Health Research Institute Brain and Body Donation Program of Sun City, Arizona, USA[67] (Supplementary Table 1a). The sections were incubated in a 60 °C oven overnight before staining after which they were deparaffinized in xylene and rehydrated in decreasing grades of alcohol. The sections were then stained using Leica Bond RX under standard IHC protocols within UCLA's TPCL. Briefly, automated detection was performed based on protocol F using the Bond Polymer Refine Detection kit (Leica Biosystems). Heat-induced antigen retrieval was performed using the BOND Epitope Retrieval Solution 2 (Leica Biosystems, catalogue no. AR9640) buffer for 30 min. For chromogenic IHCs, the primary CD4 (Cell Marque, 104R-14, 1:50) was incubated for 60 min. Sections were incubated with Dakocytomation Envision System Labelled Polymer HRP anti-rabbit (Agilent Technologies, catalogue no. K4003) for 10 min followed by BOND Polymer Refine Detection DAB chromogen (Leica, catalogue no. DS9800) for 10 min. Images were acquired with a Lionheart LX Automated Microscope (Agilent Technologies). In some cases, QuPath was used to view slides scanned with an Aperio ScanScope AT (Leica) in the UCLA TPCL[51]. For fluorescent IHC, the sections were blocked in 10% donkey serum, 1% BSA and 0.1% Tween in tris-buffered saline (TBS) for 30 min at room temperature, and then incubated with the primary antibodies overnight (Supplementary Table 3). The sections were washed in 0.1% Tween TBS and incubated with the secondary antibodies for 1 h at room temperature. The sections were then washed in 0.1% Tween TBS, treated with an autofluorescence quenching kit (Vector, SP-8400-15) following the manufacturer's instructions, incubated in 1:10,000 DAPI in PBS for 10 min, washed again and mounted onto slides with ProLong Glass mounting medium. Information regarding sex is included in Supplementary Table 1a; however, sex was not taken into consideration when including patient samples. Findings did not apply to only one sex.

Rotarod coordination test

All behavioural testing was performed under a handling hood with lights off. On the first day, the mice were trained on a rotarod (Ugo Basile) with a constant speed of 8 rpm for a total of 5 min. Then, on the next three consecutive days, the animals were placed on an accelerating rotarod. The speed of rotation constantly accelerated from 4 rpm to 40 rpm in 3 min, and a trial lasted for a maximum of 5 min. The time was recorded when the animal fell off the apparatus or spun on it twice without attempts to resume running (latency to fall). On each day, the animals did 2 trials with 15–25 min break, and the results are presented as the mean of latency to fall (6 trials).

Statistics

All statistical analyses were performed in Prism (GraphPad Software, v.9.3.1) or R (v.4.3.2) and a complete overview is provided in Supplemental Table 4. Outliers were identified in Fig. 1j and Extended Data Fig. 3a and removed from the dataset using GraphPad Prism (ROUT, Q = 1%). For some datasets, bimodality was observed, probably reflecting variability introduced by different researchers performing experiments on separate days (for example, Figs. 1p, 3d and 5k and Extended Data Fig. 2i). Normal distribution and equality of variance of the residuals were tested using the Shapiro–Wilk normality test and the *F*-test, Spearman's test, Bartlett's test, Brown-Forsythe test or Levene's test, using significance level $\alpha = 0.05$. To stabilize variances on heteroscedastic residuals, we performed $\log_{10}$ or square root transformations on the data for Figs. 1c, 2d,g, 3p, 4f and 5c,d,g,j,n and Extended Data Figs. 2d, 4i, 6h,l,n and 7h,j (linear data were used for plotting to facilitate interpretation of the outcome). For Fig. 1p, to test the association between two binary variables (SAA negative versus positive), the Fisher's exact test was used. A one-sample *t*-test was performed to assess whether the mean αS levels in enteric neurons (Extended Data Fig. 2l) significantly differed from zero, analysed independently for each group. Two groups were compared using two-sided unpaired Student's *t*-test, two-sided Welch's *t*-test or two-sided Mann–Whitney test, depending on the data structure. For clonotype overlap (Jaccard and Expanded Index) and effective number of species between ME and dura mater, Bonferroni-adjusted unpaired *t*-test with Welch's correction was used (Fig. 3r,t and Extended Data Fig. 5a). To compare more than two groups (IgG, anti-CSF1R, anti-CCR2 or anti-CSF1R/anti-CCR2), one-way analysis of variance (ANOVA) with Bonferroni's multiple-comparison posthoc test, Kruskal–Wallis test with Dunn's multiple comparisons posthoc test was used, depending on the data structure. Two-way ANOVA with Bonferroni's multiple-comparison test was used to assess the interaction of PD-αS versus NHC-αS injection with (1) anti-CSF1R/anti-CCR2 versus IgG treatment, (2) UV versus non-UV illumination, (3) *Cx3cr1*^{CreERT2}.*Tgfb1*^{LoxP} versus *Cx3cr1*$^{+/+}$.*Tgfb1*^{Lox} or at (4) 1 month or 3 months post-treatment. Two-way repeated measures ANOVA was used when values were matched (for example, different ME-Mac clusters or intestinal regions from the same mouse in Fig. 4f and Extended Data Figs. 2b and 6j,l; within variable, mouse). Multiple Mann–Whitney tests, with the Benjamini–Krieger–Yekutiel correction to control for the false discovery rate, were used to compare αS levels between cytosolic and insoluble fractions, as well as to compare cytokine levels in ME at 1 month postinjection. For brain region (SNpc versus VTA) versus treatment (NHC versus PD-extract injection) analysis in Fig. 2k and Extended Data Fig. 3f, we used a linear mixed-effect model with multivariate *t*-distribution posthoc (Fig. 2k), using mouse as a nested variable to incorporate the intermouse differences across region. All data are presented as mean ± s.e.m., statistical significance was set at $\alpha = 0.05$. Statistical methods were not used to predetermine study sizes but were based on similar experiments previously published. Experiments were blinded to the genotype of the animal as well as the treatment of the animal. Experiments involving human sections were blinded to the demographics of the patients. Independent experiments were performed to confirm the reproducibility of the data.

Reporting summary

Further information on research design is available in the Nature Portfolio Reporting Summary linked to this article.

Data availability

TCR raw data are available at the Sequence Read Archive, accession number PRJNA1321765. Single-cell sequencing raw data are available at the Gene Expression Omnibus, accession number GSE307000. Proteomics raw data are available at the Proteomics Identifications Database (PRIDE), accession number PXD069218. DSP data are available at Dryad (https://doi.org/10.5061/dryad.12jm63zb6)[68]. Source data are provided with this paper.

Code availability

Code for TCR analysis is available through GitHub at https://github.com/mvcowley/synucleinopathy-tcrs; code for single-cell sequencing and

Nichenet analysis is available through GitHub at https://github.com/Victor-K27/De_Schepper_etal_2025 and code for proteomic analysis is available through GitHub at https://github.com/UKDRI/Proteomics/blob/main/code%20repositories/UKDRI_DIANN_output_processing.R.

51. Bankhead, P. et al. QuPath: open source software for digital pathology image analysis. *Sci. Rep.* **7**, 16878 (2017).
52. Aron, L. et al. Pro-survival role for Parkinson's associated gene DJ-1 revealed in trophically impaired dopaminergic neurons. *PLoS Biol.* **8**, e1000349 (2010).
53. Meka, D. P. et al. Parkin cooperates with GDNF/RET signaling to prevent dopaminergic neuron degeneration. *J. Clin. Invest.* **125**, 1873–1885 (2015).
54. Kramer, E. R. et al. Absence of Ret signaling in mice causes progressive and late degeneration of the nigrostriatal system. *PLoS Biol.* **5**, 0616–0628 (2007).
55. Merritt, C. R. et al. Multiplex digital spatial profiling of proteins and RNA in fixed tissue. *Nat. Biotechnol.* **38**, 586–599 (2020).
56. Uddin, I. et al. Quantitative analysis of the T cell receptor repertoire. *Methods Enzymol.* **629**, 465–492 (2019).
57. Oakes, T. et al. Quantitative characterization of the T cell receptor repertoire of naïve and memory subsets using an integrated experimental and computational pipeline which is robust, economical, and versatile. *Front. Immunol.* **8**, 1267 (2017).
58. Peacock, T., Heather, J. M., Ronel, T. & Chain, B. Decombinator V4: An improved AIRR compliant-software package for T-cell receptor sequence annotation? *Bioinformatics* **37**, 876–878 (2021).
59. Hughes, C. S. et al. Single-pot, solid-phase-enhanced sample preparation for proteomics experiments. *Nat. Protoc.* **14**, 68–85 (2018).
60. Demichev, V., Messner, C. B., Vernardis, S. I., Lilley, K. S. & Ralser, M. DIA-NN: neural networks and interference correction enable deep proteome coverage in high throughput. *Nat. Methods* **17**, 41–44 (2019).
61. Phung, T. K. et al. CURTAIN—a unique web-based tool for exploration and sharing of MS-based proteomics data. *Proc. Natl Acad. Sci. USA* **121**, e2312676121 (2024).
62. Schafer, D. P., Lehrman, E. K., Heller, C. T. & Stevens, B. An engulfment assay: a protocol to assess interactions between CNS phagocytes and neurons. *J. Vis. Exp.* **88**, e51482 (2014).
63. Bujko, A. et al. Transcriptional and functional profiling defines human small intestinal macrophage subsets. *J. Exp. Med.* **215**, 441–458 (2017).
64. de Boni, L. et al. Brain region-specific susceptibility of Lewy body pathology in synucleinopathies is governed by α-synuclein conformations. *Acta Neuropathol.* **143**, 453–469 (2022).
65. Sanderson, J. B. et al. Analysis of α-synuclein species enriched from cerebral cortex of humans with sporadic dementia with Lewy bodies. *Brain Commun.* **2**, fcaa010 (2020).
66. Hao, Y. et al. Integrated analysis of multimodal single-cell data. *Cell* **184**, 3573–3587 (2021).
67. Beach, T. G. et al. Arizona Study of Aging and Neurodegenerative Disorders and Brain and Body Donation Program. *Neuropathology* **35**, 354 (2015).
68. De Schepper, S. et al. Intestinal macrophages modulate synucleinopathy along the gut-brain axis. *Dryad* https://doi.org/10.5061/dryad.12jm63zb6 (2025).

Acknowledgements We thank our funders: the Chan Zuckerberg Neurodegeneration Challenge Network (grant no. CZI NDCN) Collaborative Pairs (T.B. and S.H.), the UK Dementia Research Institute (grant nos. UKDRI-1011, UKDRI-1207, UKDRI-1209) (which receives its funding from UK DRI Ltd, funded by the UK Medical Research Council, Alzheimer's Society and Alzheimer's Research UK) (T.B. and S.H.). We thank the US National Institute of Neurological Disorders and Stroke grant nos. U54-NS110435, R01-NS109209 and R01-NS078165, R01-NS133979 (T.B.) and the Anonymous Foundation (S.H.). We acknowledge the Wellcome Trust Sir Henry Wellcome Fellowship (grant no. 221634/Z/20/Z) (S.D.S.) and the Wellcome Trust studentship (grant no. 219906/Z/19/Z) (G.C.). B.C. and M.V.C. were supported by a grant from the Rosetrees Trust, M.G. was supported by the Swiss National Science Foundation (grant no. 310030_184915). We thank J. Evans (FACS Core Facility at UCL, flow cytometry assistance and cell sorting). We thank A. Liston (Babraham Institute and University of Cambridge), S. Nuber (Harvard University), N. J. Jiang (University of Pennsylvania), S. Kim (Chungbuk National University), F. Tonelli and R. Nirujogi (University of Dundee) for experimental and intellectual support. We thank V. Lennon for anti-HUC/D antibody (Mayo Clinic) and M. Mack (Universität Regensburg) for MC21. We thank E. Ghiradello and P. Muckett (UK DRI at UCL; animal husbandry). We thank A. Džanko for experimental contributions. We are grateful to the Banner Sun Health Research Institute Brain and Body Donation Program of Sun City, Arizona, for the provision of human tissue and data. The Brain and Body Donation Program is supported by the National Institute of Neurological Disorders and Stroke (grant no. U24 NS072026 National Brain and Tissue Resource for Parkinsons Disease and Related Disorders), the National Institute on Aging (grant no. P30 AG19610 Arizona Alzheimers Disease Core Center), the Arizona Department of Health Services (contract no. 211002, Arizona Alzheimers Research Center), the Arizona Biomedical Research Commission (contract nos. 4001, 0011, 05-901 and 1001 to the Arizona Parkinsons Disease Consortium) and the Michael J. Fox Foundation for Parkinsons Research. We acknowledge Y. Li and the Translational Pathology Core Laboratory (TPCL) at UCLA for assistance with tissue processing, IHC staining and scanning. We are grateful to S. Byrne and G. Nageswaran from the UCL Adaptive receptor sequencing unit (https://www.innate2adaptive.uk/arrp) for carrying out the sequencing of the TCR repertoires. We thank M. Rahim for data analysis. We thank the UK DRI Core Informatics team, I. Shittu (Glia Data Wrangler), S. Abadijou (Senior Software Engineer) and A. Zadissa (Associate Director), for developing and maintaining the Neuromics Explorer (https://neuromics-explorer.ukdri.ac.uk/#visualisation---hong-lab). We are also grateful to members of the Hong and Bartels laboratories, the CZI NDCN and the International Neuroimmune Consortium for helpful discussions and critical feedback.

Author contributions S.D.S., S.H. and T.B. designed and conceptualized the study. S.D.S., J.A.C. and M.Y. performed ME αS fibril injections. S.D.S. and M.Y. performed rotarod behavioural testing. S.D.S. and D.S. performed all flow cytometry experiments. D.S. and E.J.V. performed all human tissue immunostainings. S.D.S., V.C. and D.S. performed all immunophenotyping experiments including immunostaining, flow cytometry and αS engulfment. D.S., M.V.-P. and K. M. performed dura mater immunostainings. M.V.C., B.C. and D.P. performed TCRα/β repertoire sequencing and analysis. S.D.S., B.G. and D.R.A. performed mass spectrometry and analysis. S.D.S., D.G. and V.K. performed single-cell sequencing and analysis. J.A.C. performed all stereological neuron counting experiments. S.D.S., J.A.C. and M.Y. performed αS pathology characterization. D.S. performed cytokine profiling of ME. L.Z., M.E., M.C., J.A.C. and A.W. performed fibril extraction and SAA. A.S., V.K., M.V.C. and D.G. performed software and bioinformatic analysis. S.D.S., V.K., A.S., G.C., J.A.C., M.V.C., D.G., D.S., M.Y., L.Z., M.E., M.V.-P., E.J.V., B.G., Z.B. and T.B. contributed to data analysis. S.D.S., V.K., D.G., D.S., M.Y., J.A.C., L.Z., M.V.-P., E.J.V., M.V.C., B.G., Z.B. and T.B. performed validation analysis. S.D.S., V.K., D.S., M.Y., A.W., L.Z., F.T.H. and K.M. optimized protocols. V.C., K.M., K.L., M.C., K.L., M.G., Z.J. and D.R.A. were responsible for mice and resources. S.D.S., S.H., T.B. and J.A.C. wrote the original and revised draft with input from all co-authors. D.R.A., B.C., S.H. and T.B. supervised the research and funding acquisition.

Competing interests The authors declare no competing interests.

Additional information

Supplementary information The online version contains supplementary material available at https://doi.org/10.1038/s41586-025-09984-y.

Correspondence and requests for materials should be addressed to Sebastiaan De Schepper, Soyon Hong or Tim Bartels.

Peer review information *Nature* thanks Veerle Baekelandt, Wouter Peelaerts and the other, anonymous, reviewer(s) for their contribution to the peer review of this work.

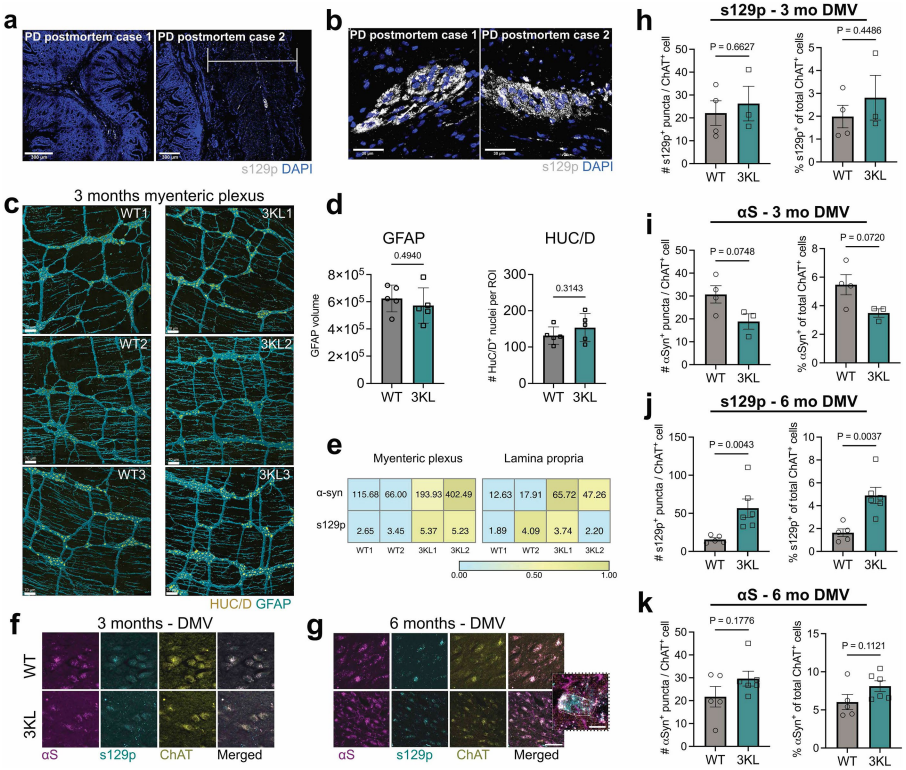

Extended Data Fig. 1 | Neural characterization of the ENS and CNS in 3KL αS transgenic mice. a,b, Confocal overview (**a**) and insert (**b**) images of s129p in ME of postmortem PD jejunum. **c,d**, Reconstructed 3D images (**c**) and quantification of myenteric GFAP and HUC/D volume (**d**) in duodenum of 3 mo WT vs 3KL, n = 5 animals/genotype and 4 ROI/ animal. 2 experiments, data analysed using unpaired t test. **e**, Heatmap showing total αS and s129p$^+$ αS levels in lamina propria and myenteric plexus of 3 mo 3KL vs WT mice, obtained by DSP. n = 2, 2–3 ROI/Mouse. **f,g**, Confocal micrographs of total αS, s129p αS and choline acetyltransferase (ChAT) in WT vs 3KL DMV at 3 mo (**f**) and 6 mo (**g**). Insert in **g** shows an individual ChAT$^+$ DMV cell. Scale bars = 50 µm, insert in **g** = 10 µm. **h-k**, quantification of punctate s129p$^+$ αS (**h,j**) or total punctate αS (**i,k**) within ChAT$^+$ DMV cells by number of puncta per ChAT$^+$ cell (left) and mean %area covered per ChAT$^+$ cell (right) of 3 mo (**h,i**) or 6 mo (**j,k**) WT vs 3KL. n = 4 mice (WT) and n = 3 mice (3KL), 53–107 ROIs per mouse (**h, i**) and n = 5 mice (WT) and n = 6 mice (3KL), 13–108 ROIs per mouse (**j,k**). 2 experiments, unpaired t test or Mann-Whitney test (**j**, left). Data are mean ± s.e.m.

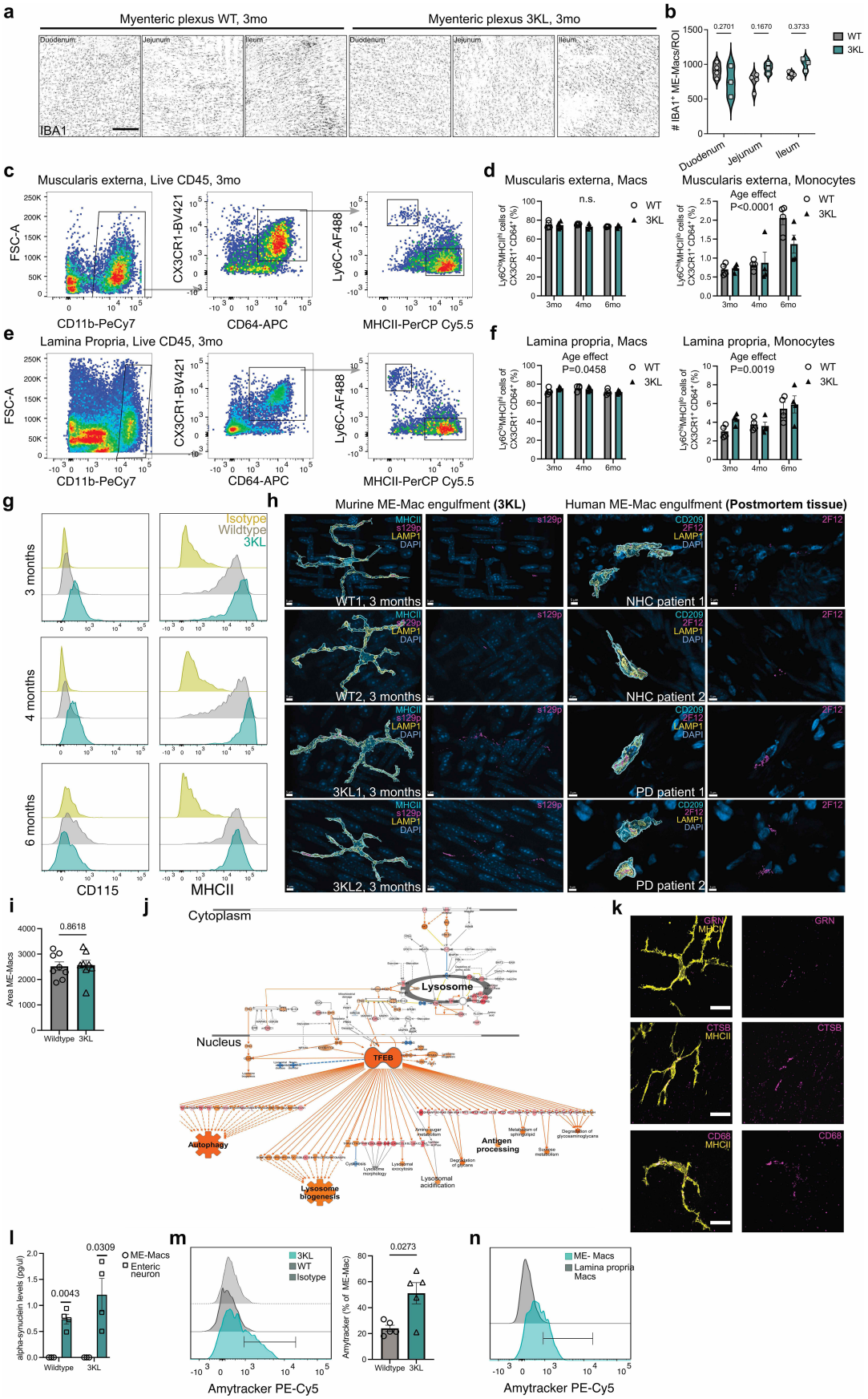

Extended Data Fig. 2 | See next page for caption.

Extended Data Fig. 2 | Characterization of ME-Macs in 3KL αS transgenic mice. a,b, Tresholded images (**a**) and manual counting (**b**) of IBA1$^+$ Macs in duodenal, jejunal and ileal myenteric plexus of 3 mo WT vs 3KL, n = 3–4 mice per group. 1 experiment, data analysed using 2way repeated measures ANOVA, Bonferroni's multiple comparison test. Scale bar = 500 µm. **c-f**, Gating strategy (**c,e**) and frequency (**d,f**) of Ly6C and MHCII by live CD11b$^+$CD64$^+$CX3CR1$^+$ cells from digested ME (**c,d**) and LP (**e,f**) of WT vs 3KL mice, n = 4 animals per age and condition. 1 experiment per age, 2way ANOVA. **g**, Histograms showing CD115 and MHCII expression in Ly6C$^-$MHCII^{hi} ME-Macs of WT vs 3KL mice. **h**, Reconstructed images of lysosomal s129p engulfment in duodenal ME-Macs of 3 mo WT vs 3KL and PD postmortem vs NHC ME. Data representative of 2 experiments. **i**, Area of 3 mo WT vs 3KL ME-Macs, calculated via 3D reconstruction, n = 8 animals per genotype. 2 experiments, unpaired t test. **j**, Pathway analysis of upregulated proteins in 3 mo WT vs 3KL ME-Macs. **k**, Confocal images of GRN, CTSB and CD68 in ME-Macs of 3 mo 3KL mice. Scale bar= 20 µm. **l**, Quantification of αS levels in isolated enteric neurons vs ME-Macs via anti- αS ELISA. n = 3 mice (ME-Mac) and n = 4 mice (enteric neurons) per genotype. Samples were normalized for total protein amount before measurement (BCA). 2 experiments, one sample t test, with comparison to a value of 0. **m,n**, Histograms showing Amytracker staining and quantification in isolated WT vs 3KL ME-Macs (**m**) and LP-Macs vs ME-Macs in 3KL ME-Macs, n = 5 animals per genotype (**n**). 1 experiment, unpaired t test with Welch's correction. Data are mean ± s.e.m.

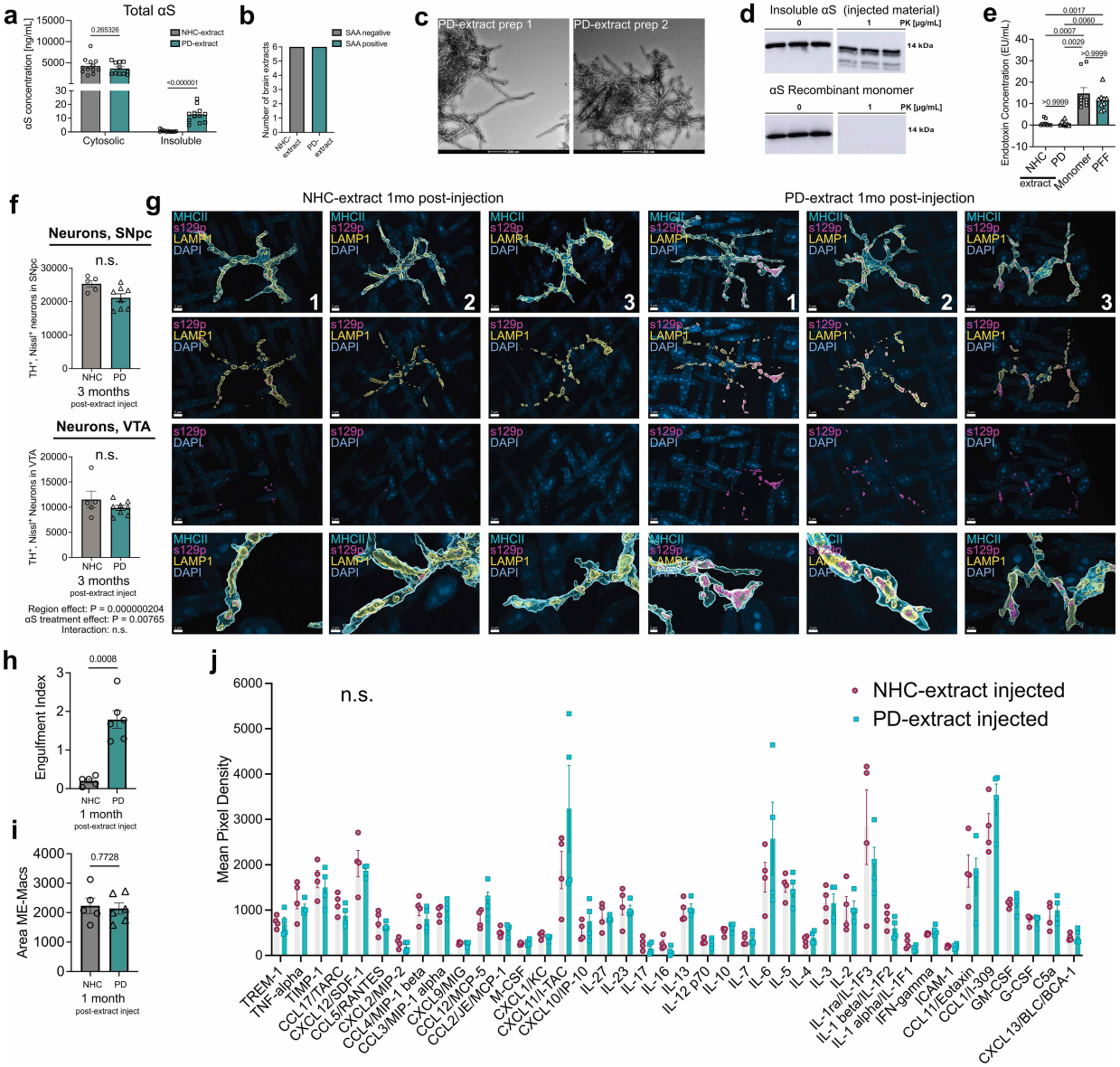

Extended Data Fig. 3 | ME-injected PD-extracts trigger macrophage uptake and propagation of αS. a, ELISA αS analysis in human brain soluble (cytosolic) and insoluble protein (used for injections) sequential extracts from frontal cortical samples of NHC vs PD patient samples. Samples were normalized for total protein amount before measurement (BCA). n = 12 per disease status and sample, data analysed using multiple Mann-Whitney tests with Benjamini-Krieger-Yekutiel to control for FDR. **b**, SAA analysis of insoluble protein extracts from NHC-αS vs PD-αS extracts. Samples with lag times <control (equal-concentration recombinant monomer) were classified as positive; those with ≥ lag times were considered negative. **c**, TEM images of PD brain insoluble preparations show the presence of amyloid fibrils. **d**, Proteinase K digest of insoluble human brain fractions shows high PK resistance of pathology associated αS in contrast to monomeric recombinant protein. Representative of 3 experiments. For gel source data, see Supplementary Fig. 1. **e**, Endotoxin concentration (EU/mL) in NHC vs. PD isolated αS fibrils samples used in gut injection models. For comparison recombinant monomer and PFF preparations at equal doses typically used in previous studies are shown. Kruskal-Wallis test, Dunn's multiple comparisons test. **f**, Unbiased stereological quantification of TH^+ $Nissl^+$ neurons, n = 5 mice for NHC-αS (SNpc and VTA) and n = 8 mice for PD-αS (SNpc and VTA). 3 experiments, linear mixed-effect model. **g-i**, Reconstructed images of lysosomal s129p engulfment in ME-Macs at 1 mo post-NHC-αS vs PD-αS injection (**g**), quantification of engulfment (**h**) and duodenal ME-Mac area (**i**), n = 5–6 per condition. 2 experiments, unpaired t test (**h**) with Welch's correction (**h**). **j**, Densitometry analysis of cytokine panel from duodenal ME lysates at 1 mo post-αS-NHC vs αS-PD injection, n = 4 per condition. 2 experiments, multiple Mann-Whitney tests with Benjamini-Krieger-Yekutiel to control for FDR. Data are mean ± s.e.m.

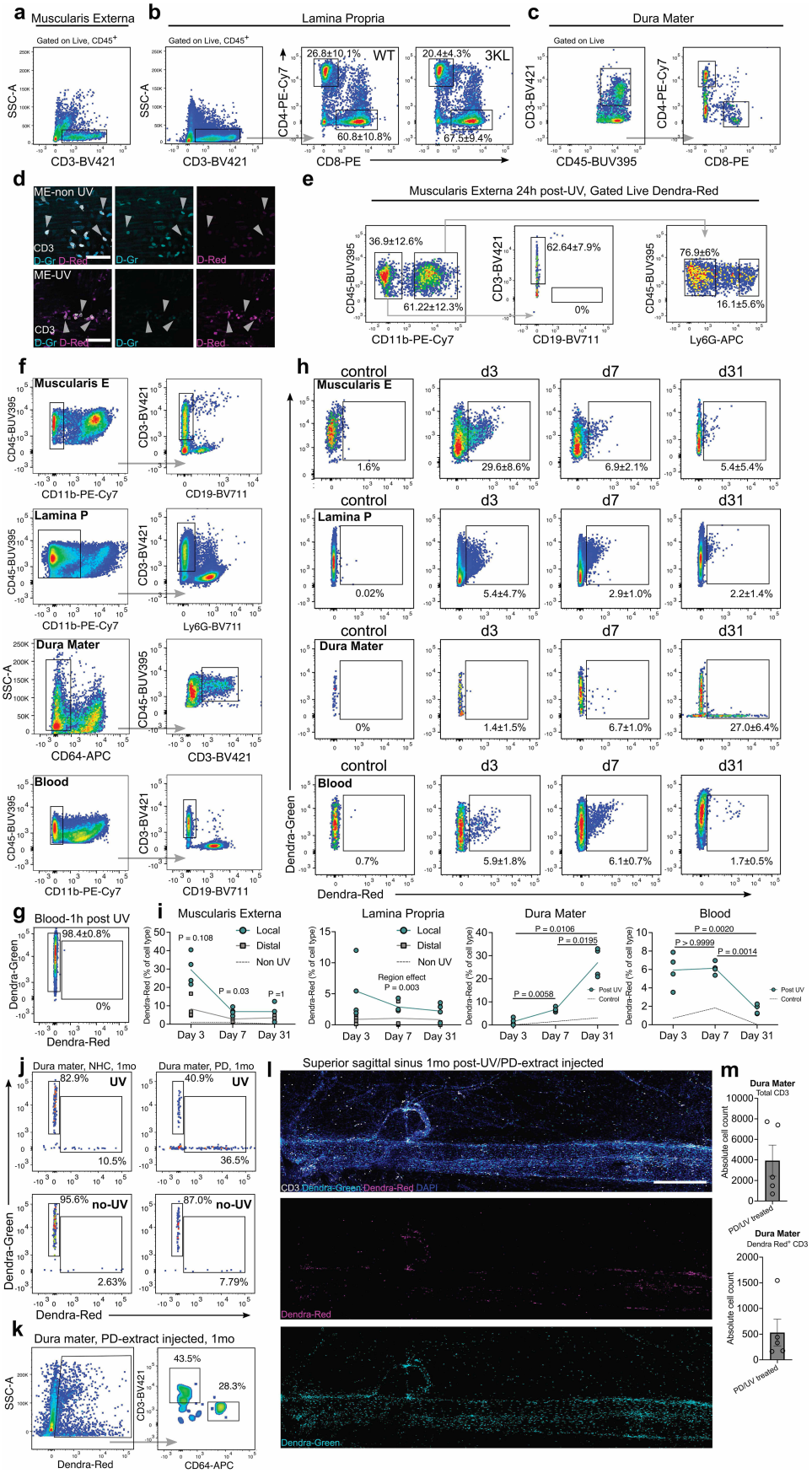

Extended Data Fig. 4 | See next page for caption.

Extended Data Fig. 4 | Characterization of T cell trafficking in the ENS and dura mater. a-c, FACS gating strategy of $CD3^+$, $CD4^+$ and $CD8^+$ cells in digested ME (**a**), LP (**b**) and dura mater (**c**) of WT vs 3KL animals. **d**, Confocal images of dendra-green vs dendra-red photoconversion in $CD3^+$ T cells in duodenal ME of Vav-H2B-Dendra2 (VHD) mice 24 h post-UV illumination vs control in ME. Scale bar = 50 µm. Representative of >2 experiments. **e**, FACS plots showing ME-Macs ($CD11b^+$ $Ly6G^-$), neutrophils ($CD11b^+$ $Ly6G^+$), T and B cells, ($CD3^+$, $CD19^+$) among dendra-red^+ cells 24 h post UV illumination. **f**, Gating strategy of $CD3^+$ T cells in ME, LP, dura mater and blood. **g**, FACS plot of dendra-red photoconversion in blood $CD3^+$ T cells, 1 h post UV illumination in ME. **h,i**, FACS plots (**h**) and frequency (**i**) of photoconverted T cells of total $CD3^+$ cells in ME, LP, dura mater and blood at d3, d7 and d31 post UV illumination vs control, n = 4 mice per time point. Mice were treated with PD-αS 3 days prior to UV illumination. Intestinal tissues were analysed at the UV-illuminated region (local) and 2 cm distal. 1 experiment, data analysed using 2way ANOVA (LP) with Bonferroni's multiple comparison test (ME), Welch's 1way ANOVA with Dunnett's multiple comparison test (Dura Mater) or 1way ANOVA with Bonferroni's multiple comparison test (blood). **j**, FACS plots of dendra-red vs dendra-green $CD3^+$ cells in dura mater at 1 mo post- PD-αS injection and UV illumination in ME. Note minor leakage in dendra-green to dendra-red photoconversion in absence of UV illumination. **k**, FACS plot of $CD3^+$ and $CD64^+$ cells among dendra-red^+ dura mater cells. **l**, Whole mount confocal image of superior sagittal sinus of dura mater, 1 mo post-PD-αS injection and UV illumination. Representative of 3 experiments. Scale bar = 1 mm. **m**, Absolute $CD3^+$ and dendra-red cell count in dura mater at 1 mo post- PD-αS injection and UV illumination in ME. n = 5 mice over 2 experiments. Data are mean ± s.e.m.

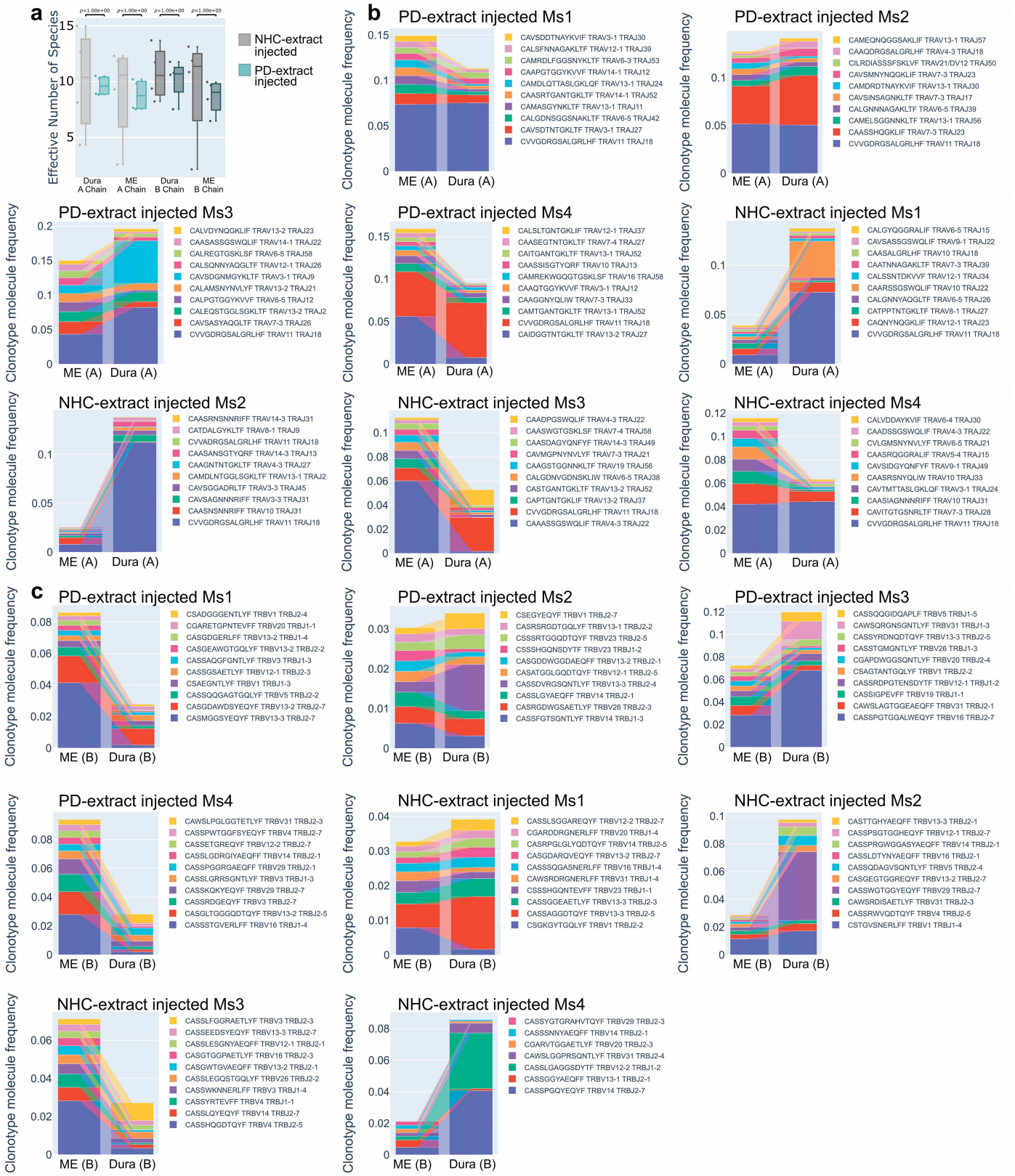

Extended Data Fig. 5 | T cell clones shared between the ME and dura mater. **a**, Boxplot quantifying the effective number of species (reciprocal of the unbiased estimator of Simpson's diversity) in the dura mater and ME of NHC-αS and PD-αS injected groups for the alpha (A) and beta (B) T cell receptor chains. Data analysed using a Bonferroni-adjusted unpaired t test with Welch's correction. Data are shown as boxplots: the median is the central line; hinges indicate the first and third quartiles; whiskers extend to the most extreme values within 1.5×IQR; and points beyond the whiskers are plotted as individual outliers. n = 4 mice per condition over 1 experiment. **b,c**, Alluvial plots of the top 10 most frequent T cell clones present in both the ME and in the dura mater of the alpha chain (**a**) and beta chain (**b**) of the PD-αS vs NHC-αS injected groups.

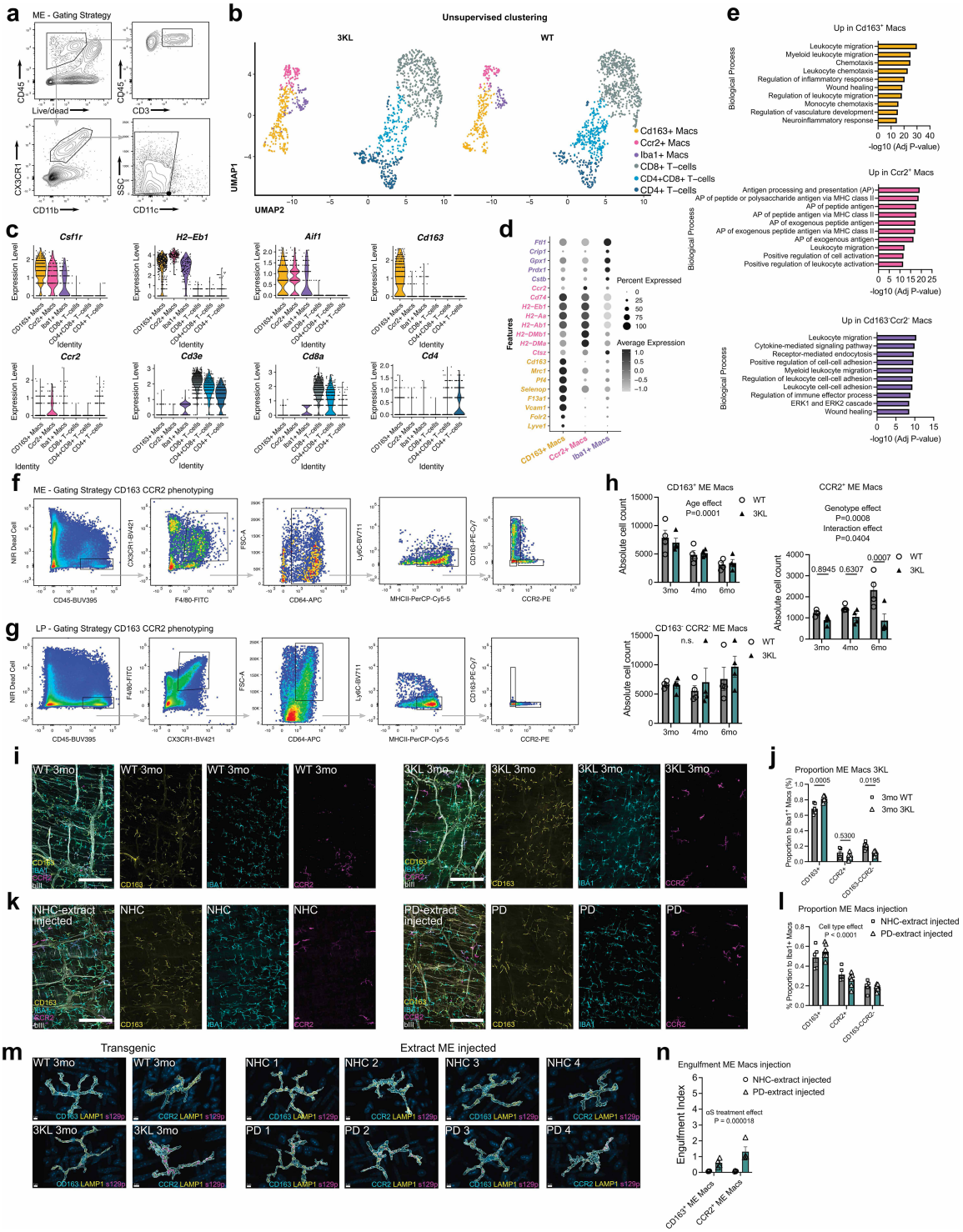

Extended Data Fig. 6 | Transcriptional and functional analysis of ME immune cells. a, FACS gating strategy of $CD3^+$ cells and $CX3CR1^{hi}CD11b^+CD11c^-$ duodenal ME-Macs. **b**, UMAP projections of 3KL vs WT ME-Macs and $CD3^+$ cells **c,d**, Violin plots (**c**) and dot plots (**d**) showing marker genes in identified ME-Mac clusters and T cells. **e**, Pathway analysis of ME-Macs of 4 mo 3KL, data analysed using a one-sided hypergeometric test. **f-g**, Gating strategy for $CCR2^+$ and $CD163^+$ ME-Macs within live $CD45^+CX3CR1^+F4/80^+CD64^+Ly6C^{lo}MHCII^{hi}$ cells in ME (**f**) and LP (**g**) and absolute cell count (**h**), n = 4 per condition and time point. 1 experiment per time point, 2way ANOVA ($CD163^+$ and $CCR2^-CD163^-$), Bonferroni's multiple comparison test ($CCR2^+$). **i-l**, Confocal images and proportion of $CCR2^+$, $CD163^+$ and $CCR2^-CD163^-$ among $IBA1^+$duodenal ME-Macs in 3 mo WT vs 3KL (**i,j**) and 1 mo post-NHC-αS vs PD-αS injection (**k,l**), n = 6 mice for WT; n = 5 mice for 3KL; n = 5 mice for NHC-αS; n = 7 for PD-αS. 3 experiments per genotype/treatment, 2way repeated measures ANOVA (**j, l**), Bonferroni's multiple comparison test (**j**). **m,n**, Reconstructed images of lysosomal s129p engulfment in $CD163^+$ and $CCR2^+$ duodenal ME-Macs at 1 mo post-αS injection and 3 mo WT vs 3KL (**m**) and quantification of engulfment at 1 mo post-αS injection (**n**), n = 4 per condition. 1 experiment, 2way ANOVA. Data are mean ± s.e.m.

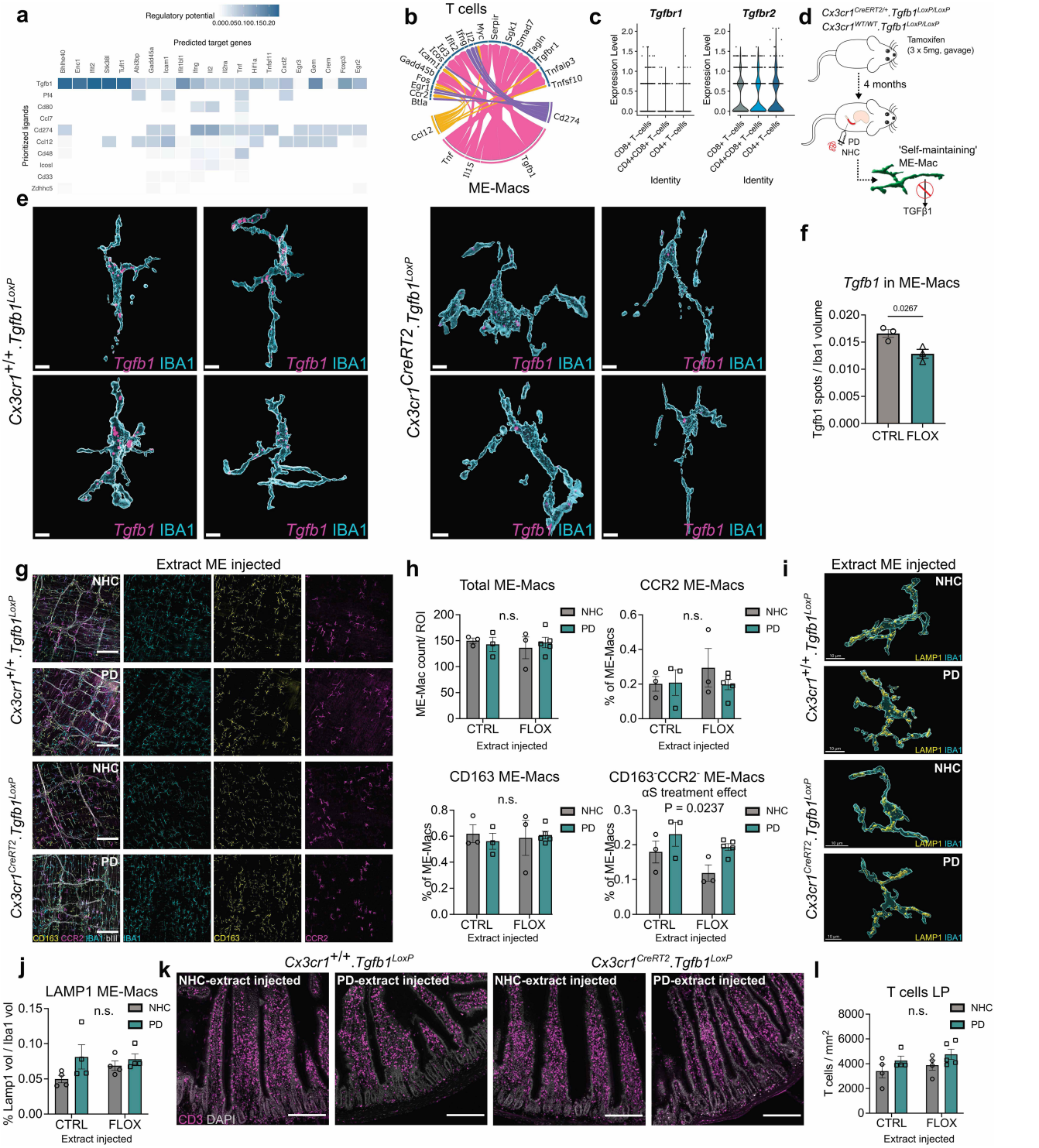

Extended Data Fig. 7 | Profiling of ME-Macs in *Cx3cr1*^{CreERT2}.*Tgfb1*^{LoxP} animals. a, Heatmap showing predicted receptor genes for represented ligands which show differential expression in ME T cells of 4 mo 3KL (receiver cells). **b**, Circos plot showing ligand-receptor pairs between ME-Macs and T cells in 4 mo 3KL. **c**, Violin plots showing *Tgfbr1* and *Tgfbr2* expression in ME T cells of 4 mo 3KL, based on our generated scRNA seq data. **d**, Schematic of *Tgfb1* depletion strategy in *self-maintaining* ME-Macs in *Cx3cr1*^{CreERT2}.*Tgfb1*^{LoxP} vs control (*Cx3cr1*$^{+/+}$.*Tgfb1*^{LoxP}) animals. **e,f**, Reconstructed images (**e**) and quantification (**f**) of duodenal ME-Macs in *Cx3cr1*^{CreERT2}.*Tgfb1*^{LoxP} vs *Cx3cr1*$^{+/+}$.*Tgfb1*^{LoxP} animals at 4 mo post-TAM treatment, n = 3 per genotype. 1 experiment, data analysed using unpaired t test. Scale bar= 5 µm. **g**, Confocal images of CD163^{+}, CCR2^{+} and CD163^{-}CCR2^{-} IBA1^{+} duodenal ME-Macs at 10 days post αS injection. Scale bar= 200 µm. **h**, Absolute count of ME-Macs and proportions of CD163^{+}, CCR2^{+} and CD163^{-}CCR2^{-} ME-Macs among IBA1^{+} ME-Macs, n = 3–5 per genotype and treatment. 1 experiment, 2way ANOVA. **i,j**, Reconstructed images of lysosomal LAMP1 in IBA1^{+} ME-Macs of *Cx3cr1*^{CreERT2}.*Tgfb1*^{LoxP} vs *Cx3cr1*$^{+/+}$.*Tgfb1*^{LoxP} animals at 4 mo post-tamoxifen treatment and 10 days post-αS injection, n = 4 per genotype and treatment. 1 experiment, 2way ANOVA. **k,l**, Confocal images (**k**) and quantification (**l**) of CD3^{+} T cells in duodenal LP of *Cx3cr1*^{CreERT2}.*Tgfb1*^{LoxP} vs *Cx3cr1*$^{+/+}$.*Tgfb1*^{LoxP} animals at 4 mo post-tamoxifen treatment and 10 days post-αS injection, n = 4 mice for CTRL (NHC- and PD-αS) and FLOX (NHC-αS); n = 5 mice for FLOX (PD-αS). 2 experiments, 2way ANOVA. Data are mean ± s.e.m.

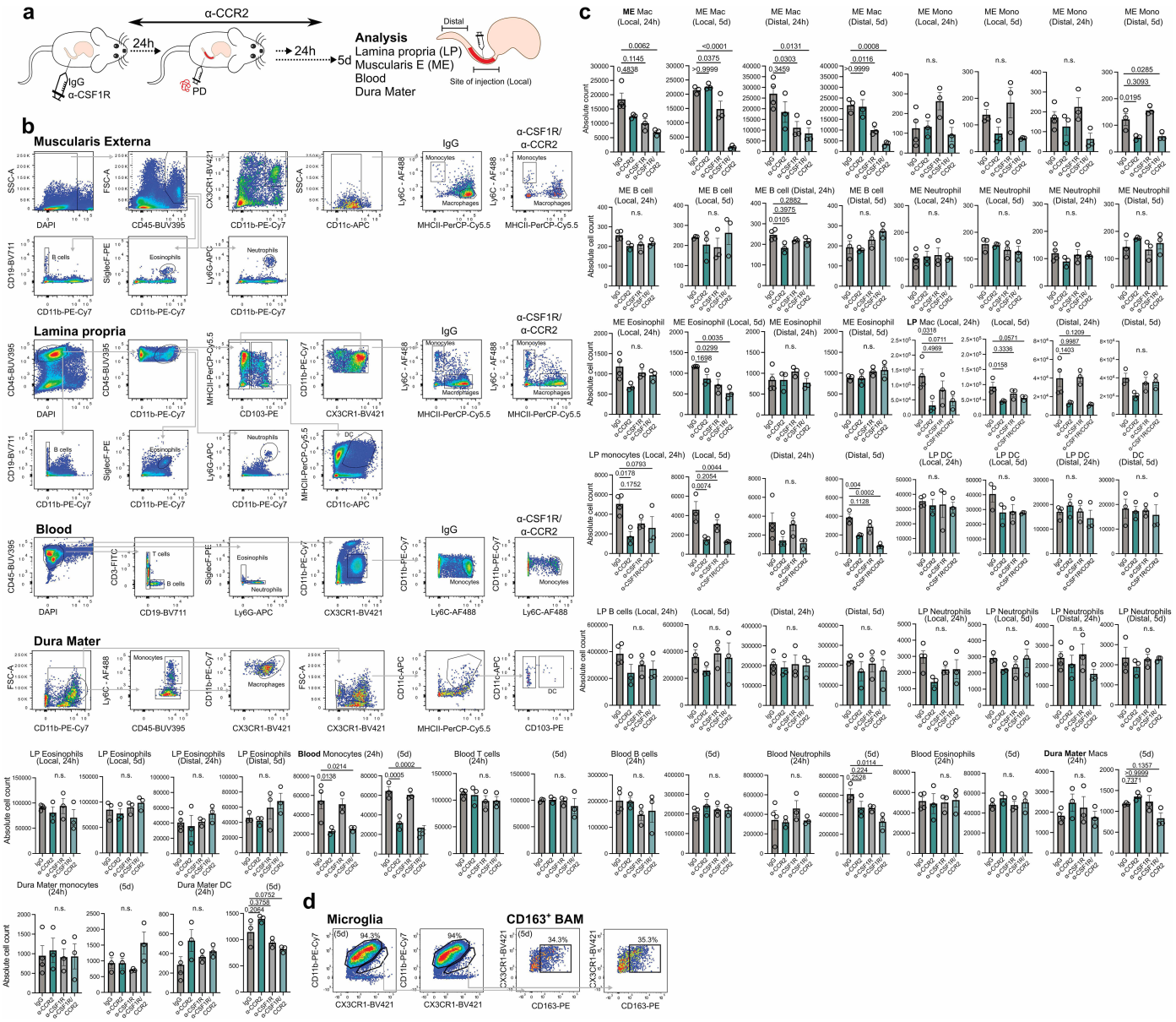

Extended Data Fig. 8 | Depletion strategy of ME-Macs. a, Schematic of α-CSF1R (AFS98) and α-CCR2 (MC21) treatment. Tissues were analysed 24 h and 5 d post-treatment, at site of injection (local) or 3 cm distant (distal). **b**, FACS gating strategy of immune cell phenotyping (macrophages, monocytes, B cells, eosinophils, neutrophils and DC) in ME, LP, blood and dura mater post- α-CSF1R/ α-CCR2 treatment vs IgG. **c**, Absolute cell counts of $CX3CR1^+CD11b^+Ly6C^{lo}MHCII^{hi}$ ME-Macs, $CX3CR1^+CD11b^+Ly6C^{hi}MHCII^{lo}$ monocytes, $CD19^+$ B cells, $CD11b^+Ly6G^+$ neutrophils, $CD11b^+SiglecF^+$ eosinophils in ME and LP; $CD11c^+CD103^+$ DC in LP; $CX3CR1^+CD11b^+Ly6C^{hi}$ monocytes, $CD3^+$ T cells, $CD19^+$ B cells, $CD11b^+Ly6G^+$ neutrophils and $CD11b^+SiglecF^+$ eosinophils in blood; $CX3CR1^+CD11b^+Ly6C^-$ macrophages, $CD11b^+Ly6C^+$ monocytes and $CD11c^+CD103^+$ DC in dura mater. n = 4 mice for IgG (except n = 3 for ME macrophages, local and distal 5 d; ME monocytes, local and distal 5 d; LP B cells and eosinophils local 5 d; ME B cells, local and distal 5 d; ME neutrophils, local and distal 5 d; LP B cells and eosinophils, distal 5 d, ME eosinophils, local and distal 5 d, LP macrophages local and distal 5 d; LP neutrophils, monocytes and dendritic cells, local 5 d; LP monocytes, dendritic cells and neutrophils, distal 5 d; blood monocytes, T cells, B cells eosinophils, neutrophils, 5 d; dura macrophages, monocytes and dendritic cells 5 d. n = 3 mice for α-CSF1R, α-CCR2 and α-CSF1R/α-CCR2 per time point. 1 experiment per time point, data analysed using 1way ANOVA with Bonferroni's multiple comparison test if applicable, Kruskal-Wallis with Dunn's multiple comparison test or Welch's 1way ANOVA with Dunnett's multiple comparison test. **d**, FACS plots of $CD11b^+CX3CR1^+$ microglia and $CD163^+$ BAM at 5 d post treatment. Data are mean ± s.e.m.

nature portfolio

Corresponding author(s): Tim Bartels, PhD
Soyon Hong, PhD
Sebastiaan De Schepper, PhD

Last updated by author(s): Nov 16, 2025

Reporting Summary

Nature Portfolio wishes to improve the reproducibility of the work that we publish. This form provides structure for consistency and transparency in reporting. For further information on Nature Portfolio policies, see our Editorial Policies and the Editorial Policy Checklist.

Statistics

For all statistical analyses, confirm that the following items are present in the figure legend, table legend, main text, or Methods section.

n/a	Confirmed	
☐	☒	The exact sample size (*n*) for each experimental group/condition, given as a discrete number and unit of measurement
☐	☒	A statement on whether measurements were taken from distinct samples or whether the same sample was measured repeatedly
☐	☒	The statistical test(s) used AND whether they are one- or two-sided *Only common tests should be described solely by name; describe more complex techniques in the Methods section.*
☐	☒	A description of all covariates tested
☐	☒	A description of any assumptions or corrections, such as tests of normality and adjustment for multiple comparisons
☐	☒	A full description of the statistical parameters including central tendency (e.g. means) or other basic estimates (e.g. regression coefficient) AND variation (e.g. standard deviation) or associated estimates of uncertainty (e.g. confidence intervals)
☐	☒	For null hypothesis testing, the test statistic (e.g. *F*, *t*, *r*) with confidence intervals, effect sizes, degrees of freedom and *P* value noted *Give P values as exact values whenever suitable.*
☒	☐	For Bayesian analysis, information on the choice of priors and Markov chain Monte Carlo settings
☒	☐	For hierarchical and complex designs, identification of the appropriate level for tests and full reporting of outcomes
☒	☐	Estimates of effect sizes (e.g. Cohen's *d*, Pearson's *r*), indicating how they were calculated

Our web collection on statistics for biologists contains articles on many of the points above.

Software and code

Policy information about availability of computer code

Data collection	FACSDiva software 4.0 (BD Biosciences) Zen Blue software Version 3.3 (Zeiss), Zen Black software Version 2.3 (Zeiss) and LAS X 5.1.0 (Leica) Cellranger count (v.6.0) QuPath (v0.5.0) StereoInvestigator Decombinator (https://zenodo.org/records/13684764)
Data analysis	Prism 9.3.1. (GraphPad Software Inc) Fiji Software 2.14.0 (NIH) and Imaris Cell Imaging Software (10.0) FlowJo 10 (Treestar) R (4.0); 10X Genomics CellRanger (version 6); Seurat (4.3); ClusterProfiler (4.12.6); Nichenetr (2.2.0). Reads were aligned using the GRCm39 (mm39) mouse genome. Python v3.12.4 Plotly v6.4.0 Scipy 1.16.2 DIA-NN version 1.8 CURTAIN version 2.0 https://curtain.proteo.info/

For manuscripts utilizing custom algorithms or software that are central to the research but not yet described in published literature, software must be made available to editors and reviewers. We strongly encourage code deposition in a community repository (e.g. GitHub). See the Nature Portfolio guidelines for submitting code & software for further information.

Data

Policy information about availability of data

All manuscripts must include a data availability statement. This statement should provide the following information, where applicable:

- Accession codes, unique identifiers, or web links for publicly available datasets
- A description of any restrictions on data availability
- For clinical datasets or third party data, please ensure that the statement adheres to our policy

Uniprot SwissProt Mouse database
TCR raw data is available at the Sequence Read Archive (SRA), accession number PRJNA1321765. Single cell sequencing raw data is available at the Gene Expression Omnibus (GEO), accession number GSE307000. Proteomics raw data is available at the Proteomics Identifications Database (PRIDE), accession number PXD069218.

Research involving human participants, their data, or biological material

Policy information about studies with human participants or human data. See also policy information about sex, gender (identity/presentation), and sexual orientation and race, ethnicity and racism.

Reporting on sex and gender	Information regarding sex is included in Supplementary Table 1a; however, sex was not taken into consideration when including patient samples. Findings did not apply to only one sex.
Reporting on race, ethnicity, or other socially relevant groupings	N/A
Population characteristics	We refer to Supplementary Table 1 for a detailed overview
Recruitment	Samples were selected based on neuropathological examination and availability of the tissues, which is unlikely to have impacted the results and conclusions.
Ethics oversight	All tissue samples were donated with the full, informed consent. Accompanying clinical and demographic data of all cases used in this study were stored electronically in compliance with the 1998 data protection act. Ethical approval for the study was obtained from the NHS research ethics committee (NEC) and in accordance with the human tissue authority's (HTA's) code of practice and standards under license number 12198, with an approved material transfer agreement. Consent has been obtained for sharing of individual-level data. Use of TPCL-derived human tissues was approved by the University of California Los Angeles Institutional Review Board, which waived the informed consent requirement for specimens acquired from the TPCL (IRB 11-002504). Specimens were deidentified and age was provided as a 5-year age range.

Note that full information on the approval of the study protocol must also be provided in the manuscript.

Field-specific reporting

Please select the one below that is the best fit for your research. If you are not sure, read the appropriate sections before making your selection.

☒ Life sciences ☐ Behavioural & social sciences ☐ Ecological, evolutionary & environmental sciences

For a reference copy of the document with all sections, see nature.com/documents/nr-reporting-summary-flat.pdf

Life sciences study design

All studies must disclose on these points even when the disclosure is negative.

Sample size	Study sizes were based on comparable experiments previously published (for example, Kim et al 2019 Neuron, Challis et al 2020 Nat Neuro)
Data exclusions	All data points were included in the analysis. Following an outlier test, only data points that were identified as outliers based on GraphPad Prism's ROUT Q=1% function were excluded from the study.
Replication	All presented data are representative of the same experiment performed in at least 3 animals, unless otherwise stated. All experiments were replicated in at least 2 independent experiments, unless otherwise stated.
Randomization	Animals were randomly assigned to different experimental groups.
Blinding	Experiments were blinded to the genotype of the animal as well as the treatment of the animal. Experiments involving human sections were blinded to the demographics of the patients.

Reporting for specific materials, systems and methods

We require information from authors about some types of materials, experimental systems and methods used in many studies. Here, indicate whether each material, system or method listed is relevant to your study. If you are not sure if a list item applies to your research, read the appropriate section before selecting a response.

Materials & experimental systems

n/a	Involved in the study
☐	☒ Antibodies
☒	☐ Eukaryotic cell lines
☒	☐ Palaeontology and archaeology
☐	☒ Animals and other organisms
☒	☐ Clinical data
☒	☐ Dual use research of concern
☒	☐ Plants

Methods

n/a	Involved in the study
☒	☐ ChIP-seq
☐	☒ Flow cytometry
☒	☐ MRI-based neuroimaging

Antibodies

Antibodies used

For Immunohistochemistry:
anti-GFP Abcam AB13970, 1:1000
CD3 BD Pharmingen 553238 1:100
CD3 Invitrogen 16-0031-82, 1:100
CD3 Biolegend 100209, 1:100
CD3 Biolegend 100240, 1:100
CD4 Abcam AB183685, 1:100
CD4 Cell Marque 102R, 1:50
CD68 Bio-Rad MCA341R, 1:100
CTSB Cell Signaling 31718S, 1:400
GRN R&D Systems AF2557, 1:100
HuC/D Donation from Prof. V. Lennon, Mayo Clinic, 1:20000
Iba1 Abcam AB225261, 1:500
Iba1 Novus Biologicals NB100-1028, 1:500
Iba1 Synaptic Systems 234308, 1:500
LAMP1 Abcam AB25245, 1:500
LAMP1 Abcam AB208943, 1:500
MHC-II Sigma-Aldrich (Merck) MABF33, 1:500
Neun Abcam AB104225, 1:300
s129p [EP1536Y] Abcam AB51253, 1:20000
s129p [MJF-R13] Abcam AB168381, 1:1000
s129p Biolegend 825701, 1:10000
βIII tubulin Abcam AB78078, 1:300
βIII tubulin Abcam AB18207, 1:300
Ccr2 Abcam AB273050, 1:50
CD163 Invitrogen 14-1631-82, 1:300
GFAP Abcam AB4674, 1:500
CD209 (human) ThermoFisher MA5-15746, 1:500
2F12 (human) Merck MABN1817 1:1000
LAMP1 (human) Abcam AB24170, 1:500
TH ImmunoStar 22941, 1:1000
TH Abcam AB112, 1:300
ChAT Sigma-Aldrich AB144P 1:500

Invitrogen A31553 goat Alexa Fluor 405, 1:500
Invitrogen A48257 donkey Alexa Fluor 405, 1:500
Invitrogen A11016 donkey Alexa Fluor 405, 1:500
Invitrogen A11039 goat Alexa Fluor 488, 1:500
Invitrogen A11055 donkey Alexa Fluor 488, 1:500
Invitrogen A21110 goat Alexa Fluor 488, 1:500
Invitrogen A11006 goat Alexa Fluor 488, 1:500
Invitrogen A21208 donkey Alexa Fluor 488, 1:500
Invitrogen A32758 donkey Alexa Fluor 594, 1:500
Invitrogen A11076 goat Alexa Fluor 594, 1:500
Invitrogen A11014 goat Alexa Fluor 594, 1:500
Invitrogen A11037 goat Alexa Fluor 594, 1:500
Invitrogen A11007 goat Alexa Fluor 594, 1:500
Invitrogen A21235 goat Alexa Fluor 647, 1:500
Invitrogen A21245 goat Alexa Fluor 647, 1:500
Invitrogen A31573 donkey Alexa Fluor 647, 1:500
Invitrogen A21247 goat Alexa Fluor 647, 1:500
2B Scientific BA-9200 goat Biotinylated, 1:200

For flow cytometry:
CX3CR1 - BV421 Biolegend 149023 1:500

CD45 - BUV395 BD Biosciences 564279 1:400
Live fixable near IR dye 780 Invitrogen 65-0865-14 1:1000
CD3 - FITC Biolegend 100204 1:500
CD3 - FITC BD Biosciences 555274 1:500
CD8 - PE BD Biosciences 553032 1:500
Ly-6C - BV711 Biolegend 128037 1:400
Ly-6C - APC/Cy7 BD Biosciences 560596 1:100
MHC-II - PE Biolegend 107608 1:500
MHC-II - PerCP/Cy5.5 Biolegend 107626 1:300
CD11b - PE/Cy7 BD Biosciences 552850 1:50
CD11c - APC Biolegend 117310 1:100
CD115 (CSF1R) - PE BD Biosciences 565249 1:400
CD11c - APC BD Biosciences 550261 1:500
CD4 - PE/Cy7 Biolegend 100422 1:100
Amytracker 680 Ebba Biotech EBB-A680 1:1000
CD163 - PE/Cy7 Biolegend 156707 1:100
Ccr2 - PE RD Systems FAB5538P 1:500
CD64 - APC Biolegend 139306 1:200
CD3 - BV421 Biolegend 100228 1:100
CD19 - BV711 Biolegend 115555 1:100
CD19 - APC BD Biosciences 550992 1:100
Ly-6G - BV711 Biolegend 108443 1:300
Ly-6G - APC Biolegend 127613 1:300
F4/80 - FITC Biolegend 123107 1:200
SiglecF-PE Miltenyi Biotec 130-102-274 1:100
Ly-6C - AF488 Biolegend 128022 1:200
CD103 - PE BD Biosciences 566844 1:500
CD163 - PE Biolegend 156704 1:500
CD163 - PE Biolegend 155308 1:500
DAPI BD Biosciences 564907 1:10000
PerCP/Cy5.5 BD Biosciences G1118TA 1:300
PE Rat IgG2a κ Isotype Ctrl, Biolegend, 400507 1:400

Validation

All antibodies were validated by the manufacturer and came with a certificate of analysis stating that the product has met all quality control standards. The tissues and species for which the antibodies were validated are reported bellow:
anti-GFP (Abcam AB13970, validation in knockout cells)
CD3 (Invitrogen 16-0031-82, validation for IHC in T-cells in mouse spleen)
CD3 (Biolegend 100209 and Biolegend 100209, validation for IHC in T-cells in mouse thymocytes)
CD4 (Abcam AB183685, validation for IHC in mouse spleens)
CD68 (Bio-Rad MCA341R, validation for IHC in rat lymph node)
CSTB (Cell Signalling 31718S, validation for IHC in human colon)
GRN (R&D Systems AF2557, validation for IHC in mouse kidney)
Iba1 (Abcam AB225261, validation for IHC in mouse brain)
Iba1 (Novus NB100-1028, validation in knockout cells / animals)
Iba1 (Synaptic Systems 234308, validation for IHC in mouse brain)
LAMP1 (Abcam AB25245, validation for IHC in human lung)
LAMP1 (Abcam AB208943, validation for IHC in mouse kidney)
MHCII (eBioscience 14-5321-82, validation for IHC in mouse splene)
Neun (Abcam AB104225, validation for IHC in mouse brain)
s129p [EP1536Y] (Abcam AB51253, validation for IHC in mouse brain)
s129p [MJF-R13] (Abcam AB168381, validation for IHC in mouse brain)
s129p (Biolegend 825701, validation for IHC in mouse brain)
βIII (Abcam AB78078, validation for IHC in mouse brain)
βIII (Abcam AB18207, validation for IHC in mouse brain and knockout cells)
CCR2 (Abcam AB273050, validation in knockout cells / animals)
CD163 (Invitrogen 14-1631-82, validation for IHC in mouse spleen)
GFAP (Abcam AB4674, validation for IHC in mouse brain)
CD209-human (ThermoFisher MA5-15746, validation for IHC in human lymph node)
LAMP1-human (Abcam AB24170, validation for IHC in human kidney)
TH (ImmunoStar 22941, validation for IHC in human brain)
TH (Abcam AB112, validation for IHC in mouse brain)

Animals and other research organisms

Policy information about studies involving animals; ARRIVE guidelines recommended for reporting animal research, and Sex and Gender in Research

Laboratory animals

Mice were used in this study:
C57BL/6J, MGI: 3028467 (age 12 weeks - 28 weeks)
3KL Tg(Thy1-SNCA*E35K*E46K*E61K)3798Nuber, MGI: 6281748 (age 12 weeks - 24 weeks)
aSyn-GFP mice: Sncatm1.1Kluk/J, MGI: J:302425 (age 12 weeks - 28 weeks)
Vav-H2B-Dendra2 (Prof. Oliver Pabst, Aachen University) (age 12 weeks - 28 weeks)
Cx3cr1:cre-ERT2, MGI:5467985 (age 30 weeks)

	Tgfb1Loxp, MGI:6331235 (age 30 weeks)
Wild animals	No wild animals were used in this study.
Reporting on sex	Both male and female mice were used in this study.
Field-collected samples	No field collected samples were used in this study.
Ethics oversight	All experiments were performed in accordance with the UK Animal (Scientific Procedures) Act, 1986 and following local ethical advice. Experimental procedures were approved by the UK Home Office and ethical approval was granted through consultation with veterinary staff at University College London (UCL).

Note that full information on the approval of the study protocol must also be provided in the manuscript.

Plants

Seed stocks	N/A
Novel plant genotypes	N/A
Authentication	N/A

Flow Cytometry

Plots

Confirm that:

☒ The axis labels state the marker and fluorochrome used (e.g. CD4-FITC).

☒ The axis scales are clearly visible. Include numbers along axes only for bottom left plot of group (a 'group' is an analysis of identical markers).

☒ All plots are contour plots with outliers or pseudocolor plots.

☒ A numerical value for number of cells or percentage (with statistics) is provided.

Methodology

Sample preparation	Mice were anesthetised using pentobarbital and were transcardially perfused with 15 mL of ice-cold filtered PBS. Collected tissues were stored in ice-cold RPMI-1640 (Gibco) completed with 5% FBS (Gibco) and 20mM HEPES (Gibco). ME: To obtain single cell suspensions, peeled ME was cut in 1-2 mm pieces and digested with 2 mg/mL Collagenase type IV and 0.8 mg/mL dispase in RPMI (Gibco) supplemented with 2% HEPES (Gibco), 2% FBS (Gibco), and 50µg/mL DNase for 1h at 37°C with continuous agitation. The single cell suspensions were then homogenised with a potter grinder and strained through 70 µm cell strainers (BD Falcon). LP: The remaining tissue following isolation of the ME, containing the lamina propria and submucosa layers, was washed with ice-cold HBSS (Gibco) supplemented with mM DTT (Sigma-Aldrich), 1 mM EDTA (Invitrogen), and 20 mM HEPES for 8 min. Single cell suspensions of LP were prepared by digestion with 0.85 mg/mL Collagenase Type V (Sigma-Aldrich) in MEMα (Lonza) supplemented with 2% HEPES, β-mercaptoethanol (Gibco) and DNase for 30 min at 37°C with continuous agitation. Brain and dura: Brains were quickly isolated from the skull, and brainstem was dissected from the rest of the brain tissue on ice using chilled instruments. The dorsal part of the skull was carefully removed and meningeal dura mater was peeled off of the skull cap. The tissues were finely chopped using chilled razorblades and transferred to tubes containing ice-cold RPMI-1640 supplemented with 10% FBS and 20mM HEPES medium. Single-cell suspensions from brainstem were prepared using the Dissociation kit (Miltenyi Biotech) according to the manufacturer's instructions and 63. Tissue chunks were pelleted by centrifugation at 300g for 2 min at 4°C followed by medium removal and resuspension in a mix of buffer Z with enzymes A, P and Y. For digestion of meningeal dura mater, chopped tissue was resuspended in 0.5 mg/mL Collagenase P, 0.8 mg/mL Dispase II and 250 U/mL DNAse1 and digested for 30 min. Single cell suspensions from all tissues were then blocked with rat anti-mouse CD16/CD32 antibodies (BD Biosciences) used at the recommended dilution for 12 min before incubation with primary antibodies diluted at recommended dilutions in FACS buffer (PBS, 2% FBS, 0.78 mM EDTA) containing Fc block for 20 min at 4°C. Dead cells were excluded using Live/Dead near-IR dye staining (Invitrogen) diluted in PBS or DAPI. Precision Count Beads (BioLegend) were used for absolute cell counting and analysed using the following formula: absolute cell count (cells/ µm) = cell count/beads count * bead concentration. Flow cytometry data were analysed using FACSDiva software (v4.0) and FlowJo software (Treestar). Cell sorting was performed on a BD Aria III (BD Biosciences). For scRNAseq (Fig. 4) and proteomics (Fig. 1), live CX3CR1hiCD11bposCD11c- ME-Macs and CD3+ cells (Extended Data Fig. 6a) were sorted in DMEM supplemented with 30% FBS and resuspended in PBS with 0.04% BSA.
Instrument	BD LSRFortessa™ X-20 Cell Analyzer (for flow cytometric analysis of cells) and BD FACSAria™ II (for cell sorting)

Software	BD FACSDiva™ Software v4.0 FlowJo™ v10
Cell population abundance	Single-cell suspensions were incubated with DAPI or Fixable Viability Dye eFluor 780 to exclude dead cells. Positive populations were gated based on negative control staining. In general, populations are given as a percentage of live, CD45+ cells, or as absolute cell numbers, unless otherwise stated.
Gating strategy	All cell populations were gated as single, liver cells, determined by FSC-A /FSC-H followed by viability dye or DAPI -negative staining. Muscularis Externa and Lamina Propria macrophages: gated as CD11b+, CX3CR1+CD64+, LY6C-MHC-II+. Muscularis Externa and Lamina Propria monocytes: gated as CD11b+, CX3CR1+CD64+, MHC-II-LY6C+. Muscularis Externa, Lamina Propria, and Dura matter T-cells: gated as CD3+, CD4+ or CD8+ (followed by Dendra green / Dendra red gating where applicable). Single cell sorting strategy: CD3+ (T-cells) or CX3CR1+CD11b+CD11c- (macrophages). Muscularis Externa and Lamina Propria CD163+/CCR2+ macrophages: gated as F4/80+CX3CR1+, CD64+, LY6C-MHC-II+, CCR2-CD163+ or CD163-CCR2+ accordingly. Muscularis Externa and Lamina Propria B-cells, Eosinophils, and Neutrophils: CD19+, CD11b+SiglecF+, and Ly6G+CD11b+ respectively. Lamina Propria Dendritic cells: CD11b+CD103+MHC-II+CD11c+. Blood T-cells, B-cells, eosinophils, neutrophils, and monocytes: CD3+, CD19+, SiglecF+, LY6G+, and CX3CR1+CD11b+LY6C+ respectively. Dura matter monocytes, macrophages, and dendritic cells: CD11b+LY6C+, CD11b+LY6C-CX3CR1+ and CD11b+CX3CR1+CD11c+MHC-II+ respectively. Brain microglia and border-associated macrophages: CD11b+CX3CR1+ and CD11b+CX3CR1+CD163+ respectively.

☒ Tick this box to confirm that a figure exemplifying the gating strategy is provided in the Supplementary Information.